Physics of structural colors

2008 Rep. Prog. Phys. 71 076401

(http://iopscience.iop.org/0034-4885/71/7/076401)

IOP PUBLISHING REPORTS ON PROGRESS IN PHYSICS

Rep. Prog. Phys. **71** (2008) 076401 (30pp) doi:10.1088/0034-4885/71/7/076401

Physics of structural colors

S Kinoshita, S Yoshioka and J Miyazaki

Graduate School of Frontier Biosciences, Osaka University, Suita, Osaka 565-0871, Japan

E-mail: skino@fbs.osaka-u.ac.jp

Received 3 September 2007, in final form 16 January 2008
Published 6 June 2008
Online at stacks.iop.org/RoPP/71/076401

Abstract

In recent years, structural colors have attracted great attention in a wide variety of research fields. This is because they are originated from complex interaction between light and sophisticated nanostructures generated in the natural world. In addition, their inherent regular structures are one of the most conspicuous examples of non-equilibrium order formation. Structural colors are deeply connected with recent rapidly growing fields of photonics and have been extensively studied to clarify their peculiar optical phenomena. Their mechanisms are, in principle, of a purely physical origin, which differs considerably from the ordinary coloration mechanisms such as in pigments, dyes and metals, where the colors are produced by virtue of the energy consumption of light. It is generally recognized that structural colors are mainly based on several elementary optical processes including thin-layer interference, diffraction grating, light scattering, photonic crystals and so on. However, in nature, these processes are somehow mixed together to produce complex optical phenomena. In many cases, they are combined with the irregularity of the structure to produce the diffusive nature of the reflected light, while in some cases they are accompanied by large-scale structures to generate the macroscopic effect on the coloration. Further, it is well known that structural colors cooperate with pigmentary colors to enhance or to reduce the brilliancy and to produce special effects. Thus, structure-based optical phenomena in nature appear to be quite multi-functional, the variety of which is far beyond our understanding. In this article, we overview these phenomena appearing particularly in the diversity of the animal world, to shed light on this rapidly developing research field.

(Some figures in this article are in colour only in the electronic version)

This article was invited by Professor Y Hirayama

Contents

1. Introduction

In nature, tremendous numbers of orders and patterns are generated spontaneously, which enliven our surroundings. One of the most remarkable consequences of these processes reveals itself as so-called *structural color*, which exhibits striking brilliancy owing to elaborate structures furnished with living creatures. They sometimes reflect surprisingly intense light in a wide angular range, while in other cases prohibit any reflection of light. These functions are natural consequences of complicated interactions between light and the structures through purely physical properties of light.

The scientific definition of structural color has not yet been settled and its characteristics are often referred to in contrast to pigmentary color. When a substance is illuminated with white light, we see a specific color if the reflected light of only a particular wavelength range is visible to our eyes. There are two ways to eliminate the other wavelengths of light: one is the case where the light is absorbed in a material, which is usually the case for ordinary coloration mechanisms in colored materials such as in pigments, dyes and metals. In these materials, the illuminating light interacts with electrons and excites them to higher excited states by virtue of the energy consumption of light. The color in this case is anyway caused by the exchange of energies between light and the electrons.

The other is the case where light is reflected and/or deflected from reaching the eyes owing to the presence of structure. The coloration in this case is based on a purely physical operation of light that interacts with various types of spatial inhomogeneity. Thus, it does not essentially involve loss of light energy. In this sense, fundamental optical processes such as reflection, refraction, interference, diffraction and scattering can become sources of structural colors. In fact, even a simple prism should be categorized into this type of structural color, because the light waves with different wavelengths are deflected differently by virtue of its wavelength-dependent refractive index. In general, the mechanisms of structural colors are categorized into several optical phenomena such as thin-film interference, multilayer interference, diffraction grating and photonic crystals. However, most of the structural colors appearing in nature somehow utilize special mechanisms to enhance the colorations by combining these optical phenomena. *Structural color* and *iridescence* are two major keywords for these phenomena and seem to be used widely in an equivalent sense. However, the term iridescence should be used somewhat in a restricted sense when the color apparently changes with the viewing angle. For example, thin-film interference is generally iridescent, while light scattering is usually non-iridescent but of a structural origin.

In this paper, we describe a wide variety of structural colors occurring in nature and attempt to clarify their underlying physics, although many of them are not fully clarified. Since a lot of excellent reviews from various viewpoints have been published recently [1–6], we prefer to place our standpoint on the physics and engineering, and overview a variety of elaborate structures in nature, particularly those in the animal world created through the evolutionary process. In the following, we place special stress on their mechanisms, especially on thin-layer interference, photonic crystals and non-iridescent mechanisms of recently growing interest. This paper is organized as follows. In section 2, we describe the historical works on structural colors that began with the observations by Hooke and Newton in the 17th century, which were then succeeded by Lord Rayleigh and Michelson, and flourishes nowadays in various scientific and industrial fields. In section 3, we present a brief description of structure-based properties of light, which appear as actual forms in various living creatures after a variety of modifications. In section 4, we show a stream of the research on structural colors in *Morpho* butterflies as a typical example. Then in section 5, various examples of structural colors in animals are presented with their up-to-date research. Finally, in section 6, we discuss the physical basis for the color-producing structures viewed from a hierarchical aspect and from the formation mechanism.

2. Historical review

The study of structural colors has a long history. Probably the oldest scientific description of structural color is found in '*Micrographia*' written by Hooke in 1665 [7]. In this book, he described the microscopic observation of the brilliant feathers of peacocks and ducks, and found that their colors were destroyed by a drop of water. He speculated that alternate layers of thin plate and air might strongly reflect the light. Newton described in '*Opticks*' that the colors of the iridescent peacock arose from the thinness of the transparent part of the feathers [8]. In spite of these pioneering works on structural colorations, further scientific development had to wait for the establishment of electromagnetic theory by Maxwell in 1873 and also for the experimental study of electromagnetic waves by Hertz in 1884. The fundamental properties of light such as reflection, refraction, interference and diffraction could be quantitatively treated thereafter and the studies on structural colors proceeded quite rapidly.

However, there arose a significant conflict between two hypotheses. One is *surface-color*, which was proposed by Walter in 1895 (see [9]) and was thought to originate from the reflection at a surface involving pigments. The other was *structure-color* that originated purely from the physical operation of light. These two hypotheses split the world of physics into two at that time. Walter explained the variation of colors with the incident angle of light as due to the change in polarization in the reflection at the absorption band edge. The idea of surface-color was then succeeded by Michelson [10], who conducted experiments on the reflectivity of seemingly metallic samples such as the golden scarab beetle and the *Morpho* butterfly, and described that they resembled the surface reflection from a very thin surface layer involving dye.

Lord Rayleigh, on the other hand, derived a formula to express the reflection properties from a regularly stratified medium using electromagnetic theory [11], and considered it as the origin of the colors of twin crystals, old decomposed glass and probably those of some beetles and butterflies. He

overviewed the studies performed so far, and explained that the brilliant colors, which varied considerably with the incident angle of light, were not due to the ordinary operation of dyes, but came from structural colors [9].

Many experimental works were performed, on an optical microscopic level, to clarify the relationship between brilliant colors and the microstructures at the surface of iridescent, metallic and whitish materials. Onslow [12] observed more than 50 iridescent animals to settle the conflict between these hypotheses. Merritt [13] measured the reflection spectra of tempered steel and the *Morpho* butterfly and interpreted them in terms of thin-layer interference. In 1924–27, Mason [14–18] published a series of papers on various types of color-producing structures in animals investigated by a microscope and supported the interference theory. Thus the interference of light gained power gradually, which kept away the interest of physicists.

Complete understanding of their structures was made after the invention of the electron microscope. In 1939, the first attempt was made by Frank and Ruska [19] to clarify the mechanism of the blue coloring in the feathers of ivory-breasted pitta using the first marketable electron microscope developed in that year. The first observation of the color-producing structures on the famous *Morpho* butterfly was reported in 1942 by Anderson and Richards [20], and by Gentil [21]. These observations revealed a surprisingly complicated structure on a tiny scale of the butterfly wing, which accelerated structural studies at the nanometre level. Many biologists attempted to elucidate the structures causing iridescence and accumulated an enormous amount of data. In 1960, a sophisticated microstructure was reported for the feather of a humming bird [22]. Thereafter, beautiful microstructures were revealed one after another in many species of birds such as peacocks, humming birds, pheasants and doves. In 1967, structural coloration due to a helicoidal structure analogous to cholesteric liquid crystals was found in the scarabaeid beetle [23]. Beautiful multilayered structure was found in a kind of jewel beetle in 1972 [24]. Highly reflecting structures were found in the 1960s within the integuments and eyes of fish and cephalopods, which are now known as animal reflectors [25]. On the other hand, regular modification of the surface was discovered to cause the anti-reflection effect, which is well-known as the moth-eye structure [26]. The motile nature of the iridescent cell in fish to ambient illumination was discovered in 1982, which was due to a change in the distance between adjacent regularly arranged platelets [27].

On the other hand, developmental studies concerning the formation of such microstructures are quite limited even up to now. Good examples for these studies are those in the butterfly scale and the multilayered structure in the beetle. Ghiradella reported a comprehensive study on the formation process of butterfly nanostructures within a scale-forming cell using an electron microscope [28–30]. Schultz and Rankin [31] reported the development of multilayer structure before and after ecdysis of the beetle.

In spite of the progress of the structural studies in biology, the physical interpretation of structural colors has not essentially progressed since Lord Rayleigh proposed multilayer interference. Only recently, structural colors have been subject to extensive studies because their applications have been rapidly growing in many industrial fields related to vision such as painting, automobiles, cosmetics, display technologies and textiles. It was soon noticed that simple interference theory no longer reproduces the actual appearance of the natural color. Furthermore, the recent research has revealed that even a very simple structure in nature has surprising multiple functions, which by far exceed our expectations. In the following, we show the beautiful microstructures produced in the natural world and give a physical basis for their optical operation.

3. Typical optical processes producing structural colors

3.1. Thin-film interference

In this section, we describe typical optical processes related to structural colors for better understanding of these marvelous phenomena. We first consider a case of thin-film interference. Let a plane wave of light be incident on a thin film of thickness d and refractive index n_b with the angles of incidence and refraction as θ_a and θ_b (figure 1(*a*)). The light reflected at the two surfaces interferes with each other. In general, the interference condition differs according to whether the thin film is attached to a material having a higher refractive index or not. The former is the case for the anti-reflective coating on glasses, while a typical example of the latter is a soap bubble. The reason for the difference is that the reflection at a surface changes its phase by 180°, when the light is incident from a material with a smaller refractive index to that with a higher one, while it does not in the inverse case.

In the soap-bubble case, the condition for constructive interference becomes

$$2n_b d\cos\theta_b = (m - 1/2)\,\lambda, \tag{1}$$

where λ is the wavelength giving the maximum reflectivity and m is an integer. On the other hand, absolutely the same condition is applied to the anti-reflective coating where destructive interference occurs. The constructive interference in the latter case is obtained simply as

$$2n_b d\cos\theta_b = m\lambda. \tag{2}$$

In this treatment, we usually consider only one-time reflection at each surface. However, when the material shows higher reflectance at the interface, multiple reflections considerably affect the interference. An exact calculation considering such multiple reflections gives the amplitude reflectivity and transmittance as

$$r = r_{ab} + t_{ab}r_{bc}t_{ba}\mathrm{e}^{\mathrm{i}\phi} + \cdots = r_{ab} + t_{ab}r_{bc}t_{ba}\mathrm{e}^{\mathrm{i}\phi}\kappa, \tag{3}$$

$$t = t_{ab}t_{bc}\mathrm{e}^{\mathrm{i}\phi/2} + t_{ab}r_{bc}r_{ba}t_{bc}\mathrm{e}^{3\mathrm{i}\phi/2} + \cdots = t_{ab}t_{bc}\mathrm{e}^{\mathrm{i}\phi/2}\kappa, \tag{4}$$

where $\kappa = 1/(1 - r_{bc}r_{ba}\exp[\mathrm{i}\phi])$ and $\phi = 4\pi n_b d\cos\theta_b/\lambda$. r_{ab} and t_{ab} are the amplitude reflectivity and transmittance at an interface incident from a to b, respectively, and are

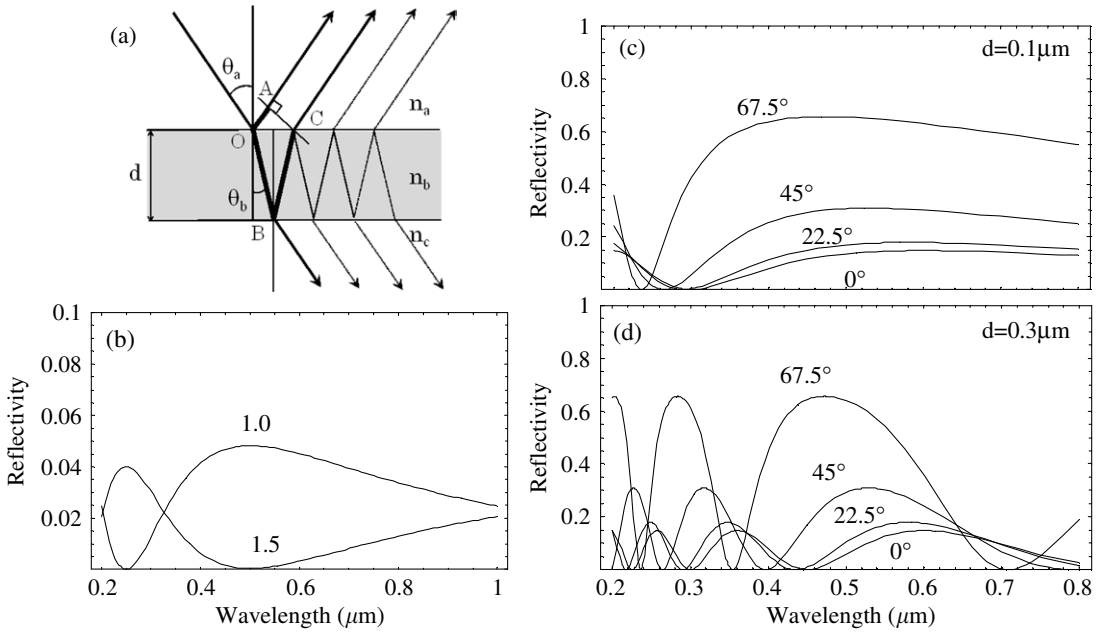

Figure 1. (*a*) Schematic diagram of thin-film interference. (*b*) Reflection properties of thin-film interference. The refractive index and thickness of the film are set at 1.25 and 0.1 μm. The film is assumed to be in contact with air ($n = 1.0$) or a material ($n = 1.5$). (*c*) and (*d*) The reflectivity from a film ($n = 1.5$) in air for various angles of incidence with the polarization direction perpendicular to the incident plane. The thicknesses of the film are assumed to be (*c*) 0.1 μm and (*d*) 0.3 μm, respectively.

obtained from Fresnel's law. Then, the power reflectivity and transmittance are given as $R = |r|^2$ and $T = (n_c/n_a)|t|^2$ with $R + T = 1$ as long as the refractive indices are real. It is easily shown that $\kappa = 1$ with $t_{ab}t_{ba} = 1$ and $|r_{ab}| = |r_{bc}|$ corresponds to one-time reflection at each surface.

The typical examples calculated for the cases of a soap-bubble and an anti-reflective coating are shown in figure 1(*b*), where we set the parameters such that constructive interference occurs at $\lambda = 500$ nm with $m = 1$. It is clear that the reflectivity is rather low in each case and smoothly changes with the wavelength. Thus simple thin-film interference gives only weak dependence on the wavelength with low reflectance. The incidence-angle dependence is shown in figure 1(*c*). Since the reflectivity at an interface is rapidly increased as the incident angle is increased, the reflection due to thin-film interference is more clearly perceptible at large angles. However, since the reflection spectrum is broad and is only weakly dependent on the incidence angle, the impression to the eye is obscure.

To enhance the reflectivity, it is necessary to increase the reflectivity at each interface. To realize this, a material having a higher refractive index such as TiO_2 is often employed. 'interference pearl luster pigment' is one such example. This coloring material involves a thin silica flake with both surfaces coated with TiO_2. The thickness of the coating is adjusted so that thin-film interference occurs efficiently. Since the reflectance is small even in this case, multiple reflection from flakes in different depths of the painting gives the pearl-like impression. When the reflectivity at the surfaces increases much more, the thin-film interference can be regarded as a kind of Fabry–Perot interferometer, because multiple reflections at both surfaces occur efficiently. Using the relation given above (equation (3)), we calculate the reflectivity with changing

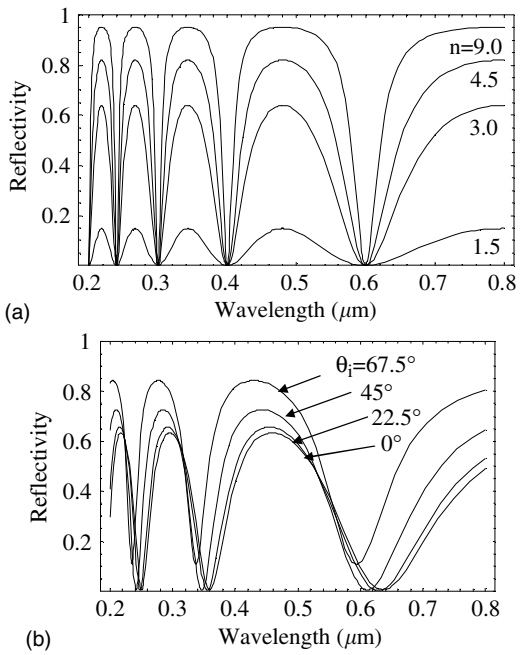

Figure 2. (*a*) Reflection properties of thin-film interference in air for materials with various refractive indices. The thickness of the material is so chosen that the optical path length becomes 0.6 μm. (*b*) Reflectivity from a metal coated by an oxide thin film, corresponding to Ti, calculated for various angles of incidence with the polarization direction perpendicular to the incident plane. The thickness and refractive index of the oxide film are set to be 0.15 μm and 2.76, respectively, while the refractive index of the metal is assumed to be 2.16+2.93i.

refractive indices of the material as shown in figure 2(*a*). At relatively low indices, low reflectivity with only weak dependence on the wavelength is observed. With increasing refractive index, the overall reflectivity is increased and tends

to be saturated. Furthermore, periodic dips appear at the wavelengths where the relation $2n_b d\cos\theta_b = m\lambda$ is satisfied. Thus to make the thin-film interference work efficiently as a coloring method, it is necessary to select appropriate reflectivity at the surfaces.

When a thin film is attached to a metal surface, similar coloration is attainable, if a proper choice of metal is made. A typical example of employing Ti metal is shown in figure 2(*b*). When the reflectivity of the metal is high enough as in the case of Al_2O_3–Al film, the total reflectivity is almost saturated and no particular coloration is expected. However, under appropriate reflectivity as in the TiO_2–Ti system, the specific coloration and iridescence are apparent. A similar effect is obtainable when a transparent material is coated by metal with appropriate thickness. These types of coloring material are called 'optically variable pigment' and are widely used in industrial applications.

If the thickness of the film becomes larger, regular multiple peaks appear in the reflection spectrum (figure 1(*d*)) as a consequence of the higher-order interference with $m > 1$. These peaks in a visible region cause a special effect called *non-spectral color* to human vision in contrast to an ordinary *spectral color*, i.e. a single wavelength of light is perceived in the eye. The non-spectral color is deeply connected with the spectral sensitivities of vision and is explained in terms that more than two color-receptors among three are sensed simultaneously. Violet is a spectral color, but purple and magenta are non-spectral colors. White is also a non-spectral color, where all three color-receptors are sensed. The multiple peak in thin-film interference can become an origin of non-spectral color. A typical example has been recently found in the neck feather of the rock dove [32, 33], which specifically shows green/purple two-color iridescence. It is expected that the angular dependence is more pronounced for the higher-order interference of $m > 1$ than that of $m = 1$ (figure 1(*d*)), which makes the iridescent effect more vivid.

3.2. Multilayer interference

Multilayer interference is qualitatively understood in terms of a pair of thin layers piling periodically. Consider two layers designated as A and B with thicknesses d_A and d_B, and refractive indices n_A and n_B, respectively, as shown in figure 3. We assume $n_A > n_B$ for the present. If we consider a certain pair of AB layers, the phases of the reflected light both at the upper and lower B–A interfaces change by 180°. Thus a relation similar to the anti-reflective coating of equation (2) is applicable as

$$2(n_A d_A \cos\theta_A + n_B d_B \cos\theta_B) = m\lambda, \qquad (5)$$

for constructive interference with the angles of refraction in the A and B layers as θ_A and θ_B. On the other hand, if we consider only the A layer within the AB layer, the phase of the reflected light does not change at an A–B interface. Thus if a soap-bubble relation, $2n_A d_A \cos\theta_A = (m' - 1/2)\lambda$, is further satisfied for the same wavelength, the reflected light from the A–B interface adds to that from the B–A interfaces and the multilayer gives the maximum reflectivity. Here, the condition

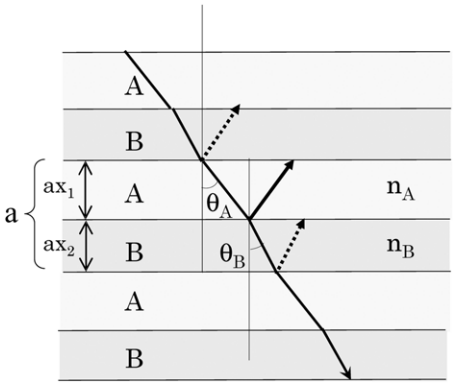

Figure 3. Schematic illustration of multilayer interference.

$m' \leqslant m$ should be satisfied because of the restriction of the thickness. In particular, the relations with $m = 1$ and $m' = 1$ correspond to the lowest-order case, where the optical path lengths, defined as the length multiplied by the refractive index, for A and B layers are equal to each other. Land called this case the *ideal multilayer* [25]. On the other hand, if the thickness of the A layer does not satisfy the soap-bubble relation, while the sum of the A and B layers satisfies equation (5), the reflection at the A–B interface works destructively and the peak reflectivity decreases. This case is the *non-ideal multilayer*.

The above interpretation, however, is too simple to understand the true mechanism of multilayer interference. It is only applicable when the difference in the refractive indices of the two layers is small enough. Otherwise, the multiple reflections modify the interference condition to a large extent. The quantitative evaluation of the wavelength-dependent reflectivity is rather complex in a general case, but is important for understanding the principle of structural colors, because most of them are originated from multilayer interference or its analogue.

The derivation of the reflectivity from a multilayer has been described frequently since Lord Rayleigh presented the paper in 1917 [11]. Nowadays, the reflectivity and transmittance of a multilayer with arbitrary refractive indices and thicknesses without any periodicity are easily calculated through a transfer matrix method [6, 34, 35], in addition to the well-known iterative and Huxley's methods [36]. Since the details of these methods have been fully described before, here we describe only the results calculated by the above methods.

First, we show the reflection spectrum for an ideal multilayer with a varying number of layers under normal incidence. In figure 4(*a*), we show the result which corresponds to the case where the difference in the refractive indices of the two layers is very small ($\Delta n = 0.05$). Since the optical path lengths of these two layers are set at 0.125 μm, the peak wavelength of the reflectivity should be 500 nm. With increasing number of layers, the peak reflectivity increases rapidly, while the bandwidth decreases gradually. Thus, in order to obtain a high reflectivity for the multilayer having small refractive-index difference, it is necessary to pile up many layers, which inevitably causes reduction of the bandwidth.

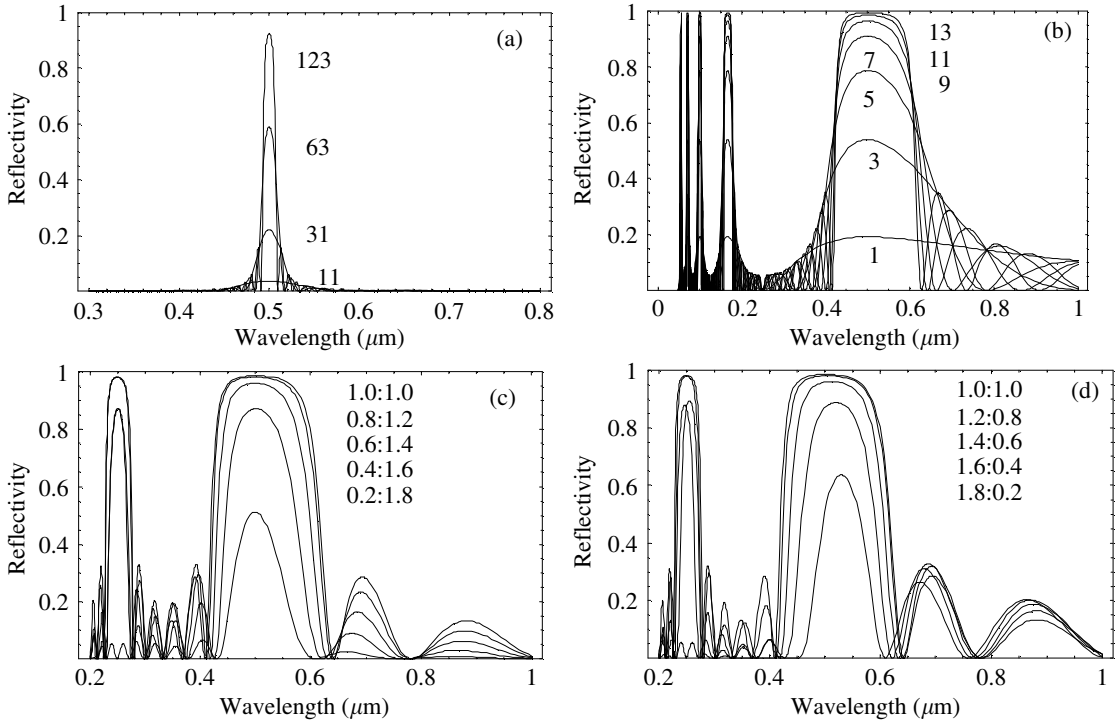

Figure 4. Reflection spectra obtained under normal incidence for ideal multilayers consisting of alternate layers with the refractive indices of (*a*) 1.6 and 1.55 embedded in a material having the index of 1.55, and (*b*) 1.6 and 1.0 in air. The thicknesses of the layers are adjusted to satisfy equation (5) for $\lambda = 0.5\,\mu$m and $m = 1$. The numbers of the layers are indicated in the figure. (*c*) and (*d*) Reflection spectra from non-ideal multilayers of 11 alternate layers corresponding to (*b*). The ratios of the optical path lengths for the high and low refractive indices are indicated in the figure. The sum of the optical path lengths for the two layers is kept constant at 0.25 μm.

In figure 4(*b*), we show the reflection spectrum of the multilayer for various numbers of layers with a difference in the refractive indices of 0.6. It is easily understood that only 11 layers are enough to make the maximum reflectivity reach almost unity. It is clear that the bandwidth in this case is considerably broader compared with that in the case of a small difference in the refractive indices.

For an ideal multilayer, the maximum reflectivity under normal incidence occurs where the relation $2n_Ad_A = 2n_Bd_B = (m' - 1/2)\lambda$ is satisfied. The amplitude reflectivity at this wavelength is obtained using a transfer matrix method as $r = (1-\gamma)/(1+\gamma)$, where γ satisfies the following relation: $\gamma = (n_t/n_i)\cdot(n_A/n_B)^N$ for N of an even number and $\gamma = n_A^2/(n_tn_i)\cdot(n_A/n_B)^{N-1}$ for N of an odd number, where we label the refractive indices of the media in the incident and transmitted spaces as n_i and n_t, respectively. Thus, for a multilayer with a large difference in n_A and n_B, the reflectivity easily reaches unity even for small N. In contrast, for the wavelength at which $2n_Ad_A = 2n_Bd_B = m\lambda$ is satisfied with m being an integer, the reflections from A–B and B–A interfaces destructively interfere. The reflectivity at this wavelength becomes $r = (n_i - n_t)/(n_i + n_t)$ and becomes null when the refractive indices of the incident and transmitted regions are the same. We can see this effect in figure 4(*b*), where the reflectivity for an even number of m disappears, while that for an odd number forms a peak.

Next, we show the result for a non-ideal multilayer. In figures 4(*c*) and (*d*), we show the calculated result corresponding to figure 4(*b*). The ratio of the optical path length of the A layer with a higher refractive index increases or decreases, while the sum of the optical path lengths of the A and B layers is kept constant. When the deviation from the ideal multilayer becomes remarkable, the bandwidth reduces drastically in addition to the decrease in the peak reflectivity. At the same time, the peak position tends to shift towards longer or shorter wavelength as the width of the A layer decreases or increases. It is also noticed that the reflectivities at the wavelengths for an even number of m restore quickly. It is clear that the simple relation of equation (5) on the analogy of thin-film interference no longer holds, since the peak wavelength shifts definitely. The shift of reflection band and its bandwidth for the lowest-order interference are generally estimated using the two-wave approximation in a one-dimensional photonic crystal, which are described in the following subsection.

3.3. Photonic crystals

If small identical particles are regularly arranged like a crystal, light scattered from each particle interferes and radiates secondary emission in regular directions. The theoretical treatment of this type of scattering was first developed in the field of x-ray diffraction, in which the theory considering only one-time scattering from each particle is called 'kinematic theory', whereas that considering multiple scattering is called 'dynamical theory'. These approaches have been extended to a system consisting of much larger particles with various crystal structures and a new research field called photonics or photonic crystals has opened. The interaction of electromagnetic waves

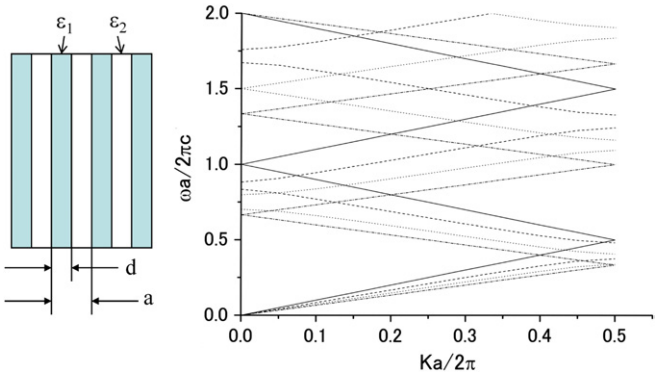

Figure 5. One-dimensional photonic crystal and its photonic band structures for $d/a = 0$, 1/3, 2/3 and 1 (from top to bottom). The permittivities, ϵ_1 and ϵ_2, are set at 2.25 and 1.0, respectively [38].

with periodic microstructures has been extensively studied in conjunction with coming new photon technology, which prevails over electronics based on semiconductor technology. However, the theoretical treatments have not been changed basically from the dynamical theory of x-ray diffraction except that accurate results are obtained through computer calculation. Detailed descriptions of photonic crystals have been amply reported [37]. In this section, we describe the optical properties of one- and two-dimensional photonic crystals, which offer a deep insight into the photonic crystals found in nature.

We first derive a general expression for the propagation of light under periodically space-modulated permittivity. Using Maxwell's equations, the electric field vector $\boldsymbol{E}(\boldsymbol{r})$ satisfies the following relation:

$$\nabla \times (\nabla \times \boldsymbol{E}(\boldsymbol{r})) = \mu_0 \epsilon(\boldsymbol{r}) \omega^2 \boldsymbol{E}(\boldsymbol{r}). \tag{6}$$

When the permittivity $\epsilon(\boldsymbol{r})$ is periodically modulated, its reciprocal can be expanded in terms of reciprocal lattice vectors $\boldsymbol{G}$s as

$$\frac{1}{\epsilon(\boldsymbol{r})} = \sum_{\boldsymbol{G}} b_{\boldsymbol{G}} \mathrm{e}^{\mathrm{i}\boldsymbol{G}\cdot\boldsymbol{r}}, \tag{7}$$

where $b_{\boldsymbol{G}}$s are the expansion coefficients. According to Bloch's theorem, the electric field under the periodic modulation on the susceptibility is also expanded in a similar manner as

$$\boldsymbol{E}(\boldsymbol{r}) = \sum_{\boldsymbol{G}} \boldsymbol{E}_{\boldsymbol{G}} \mathrm{e}^{\mathrm{i}\{(\boldsymbol{k}+\boldsymbol{G})\cdot\boldsymbol{r}-\omega t\}}. \tag{8}$$

Inserting equations (7) and (8) into equation (6) yields

$$\mu_0 \omega^2 \boldsymbol{E}_{\boldsymbol{G}} = -\sum_{\boldsymbol{G}'} b_{\boldsymbol{G}-\boldsymbol{G}'} (\boldsymbol{k}+\boldsymbol{G}') \times ((\boldsymbol{k}+\boldsymbol{G}') \times \boldsymbol{E}_{\boldsymbol{G}'}). \tag{9}$$

A set of the linear equations indexed by $\boldsymbol{G}$ gives the electric field in the modulated material.

First, we show the simplest case of one-dimensional band structure calculated by means of the plane-wave expansion method in figure 5, where we show the dispersion curves for various layer thicknesses of high permittivity keeping the period a constant. This figure corresponds to a multilayer of an infinite number of alternate layers with refractive indices of 1.5 and 1.0. At a glance, we see that the curves corresponding to $d/a = 0$ and 1 show no gap at $Ka/(2\pi) = 0.5$ that corresponds to the first Brillouin zone boundary, where $K \equiv |\boldsymbol{k}|$. This is because the multilayer is homogeneously occupied by a material of either a lower or a higher refractive index. On the other hand, the other two have a clear gap at $Ka/(2\pi) = 0.5m$, where m is an integer. It is soon understood that the gradient of a straight line starting from an origin is inversely proportional to the average refractive index in composite systems, which are exactly equal to 1.0 and 1.5 for $d/a = 0$ and 1, respectively. The concept of the average refractive index is useful because it offers an easy way to estimate the reflection band centers by extrapolating the straight line to the zone boundaries, and also offers an approximate method of analyzing the optical properties of complex structures in a long wavelength limit. The approximate expressions for the average refractive index proposed so far, such as Maxwell–Garnett and Bruggeman models, are known to give a relatively good result within the range of the linear dispersion region (see, for example [38]).

To understand the origin of the band gap in an intuitive way, it is convenient to consider the standing wave of light within a periodically modulated dielectric medium. At the first zone boundary ($Ka/(2\pi) = 0.5$), the wavelength of light is just twice the periodicity. Thus it is possible to make the wave of light match the loop (antinode) either at the layer of higher or lower permittivity. Since the electromagnetic energy is determined by the product of permittivity and the square of the electric field, the difference in the permittivity makes an energy difference between the two states, which corresponds to the energy gap. Thus, the energy gap is largest when the layer thicknesses are comparable to each other, while it becomes a minimum when either layer has extremely small thickness. This roughly explains the difference in the reflection bandwidth in ideal and non-ideal multilayers.

In order to estimate the bandwidth of the first band gap quantitatively, it is useful to consider only two relevant modes, $\omega \approx b_0 k/\sqrt{\mu_0}$ and $\omega \approx b_0 k(2\pi/a - k)/\sqrt{\mu_0}$, around $k \approx \pi/a$, as shown in figure 6. The upper and lower dispersion curves are then expressed within the second order of h [6, 37]:

$$\omega_{\pm} \approx \frac{\pi}{a\sqrt{\mu_0}} \sqrt{b_0 \pm |b_1|} + \frac{a}{2\pi\sqrt{\mu_0}\sqrt{b_0 \pm |b_1|}} \times \left(b_0 \pm \frac{2b_0^2 - |b_1|^2}{|b_1|} \right) h^2, \tag{10}$$

where we put $k = \pi/a + h$ and use the relation $b_1 b_{-1} = |b_1|^2$.

For periodic double layers, whose permittivities are expressed as $\epsilon_1 = n_1^2$ and $\epsilon_2 = n_2^2$, the expansion coefficients are simply obtained as

$$b_0 = \frac{x_1}{n_1^2} + \frac{x_2}{n_2^2},$$
$$b_1 = \frac{1}{\pi} \mathrm{e}^{-\mathrm{i}\pi x_1} \sin(\pi x_1) \left(\frac{1}{n_1^2} - \frac{1}{n_2^2} \right), \tag{11}$$

where the thicknesses of the layers, 1 and 2, are put as ax_1 and ax_2, respectively, with $x_1 + x_2 = 1$. Inserting these relations

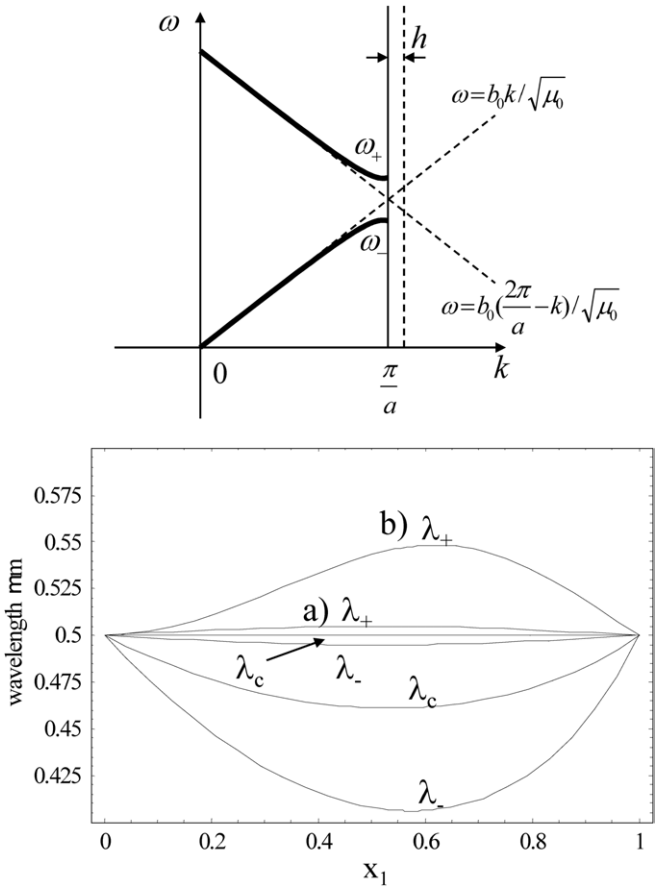

Figure 6. (Upper) Schematic band structure for an alternate multilayer near the zone boundary. (Lower) Photonic band gap for an alternate multilayer against the fraction of the layer thickness of a higher refractive index, x_1, calculated using equation (10). Light is assumed to propagate perpendicularly to the layer. The refractive indices employed are the combinations of (a) 1.6 and 1.55 and (b) 1.6 and 1.0, respectively. λ_+, λ_- and λ_c are longer and shorter wavelength edges of the band gap and its center.

into equation (10), we obtain the band center in wavelength λ_c as

$$\lambda_c = 2a \Big/ \sqrt{\frac{1}{n_2^2}\left\{1 + \frac{n_2^2 - n_1^2}{n_1^2}x_1\right\}}\,. \tag{12}$$

When $n_1 \approx n_2$, this relation reduces to

$$\lambda_c = 2a(n_1 x_1 + n_2 x_2), \tag{13}$$

which corresponds to what we have already derived in an analogy to the thin-film interference. The bandwidth is then obtained as

$$\Delta\omega \equiv \omega_+ - \omega_- \approx \frac{\pi}{a\sqrt{\mu_0}}\frac{|b_1|}{\sqrt{b_0}}, \tag{14}$$

where the last relation is derived under the assumption of $|b_1| \ll b_0$. The bandwidth in wavelength $\Delta\lambda$ is obtained as

$$\Delta\lambda = \frac{2\pi c}{\omega_-} - \frac{2\pi c}{\omega_+} = \frac{2\pi c\Delta\omega}{\omega_+\omega_-} \approx \frac{2a|b_1|}{(b_0)^{3/2}}. \tag{15}$$

Under the conditions $x_1 \approx x_2$ and $n_1 \approx n_2$, it reduces to $\Delta\lambda \approx 4a|n_2 - n_1|/\pi$. Thus the bandwidth is proportional to

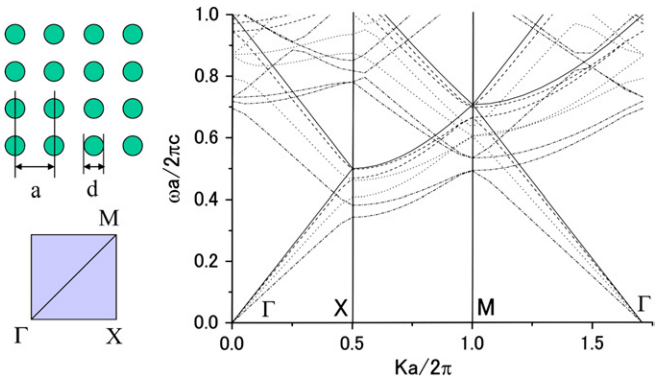

Figure 7. Two-dimensional photonic crystal and its photonic band structures for $d/a = 0$, 1/3, 2/3 and 1 (from top to bottom) in the case of p-polarization (TE). The permittivity of a cylinder is set at 2.25, while that of a medium is set at 1.0 [38].

the difference in the refractive indices of the two. In figure 6, we show the calculated results for λ_c and $\lambda_\pm(\equiv 2\pi c/\omega_\mp)$, for small and large differences in the refractive indices between the two layers. Thus the reflection bandwidths are clearly dependent on the difference in the refractive indices, which tend to be larger when the multilayer comes close to the ideal one. It is noticeable that the band center itself deviates from that determined by the volume fraction of one component, when the difference in the refractive indices is large.

In figure 7, we show the result of two-dimensional photonic crystal consisting of a square lattice of a cylinder with an infinite length. The dispersion curves between reciprocal lattice points Γ and X indicate those of light propagating along a square lattice plane, while those between Γ and M do so at 45° to this. The dispersion curves between X and M correspond to the angular change between them. It is clear that with the smallest radius of a cylinder, no gap is seen at the zone boundary. With increasing radius of the cylinder, clear gaps are seen, in addition to the decrease in the gradient of the dispersion curve near the origin. On the other hand, even for the largest radius of $d/a = 1$, a clear gap is still seen. This is because the material is not completely homogeneous since cylinders having a circular section should be packed into a square lattice.

It is generally expressed that the average refractive index obtained from the linear dispersion region in the long wavelength limit is exactly expressed by the volume averaged permittivity for s-polarization, whereas it is well expressed by the Maxwell–Garnett and Bruggeman models for p-polarization, when the difference in the permittivities is small. However, in general, it is difficult to derive the characteristic optical quantities from these figures so that the transmission/reflection spectra are often calculated numerically in a separate method.

4. Morpho butterflies

4.1. Basic descriptions of the Morpho butterflies

Before showing various color-producing structures, it is better to describe the characteristics of the *Morpho* butterflies as

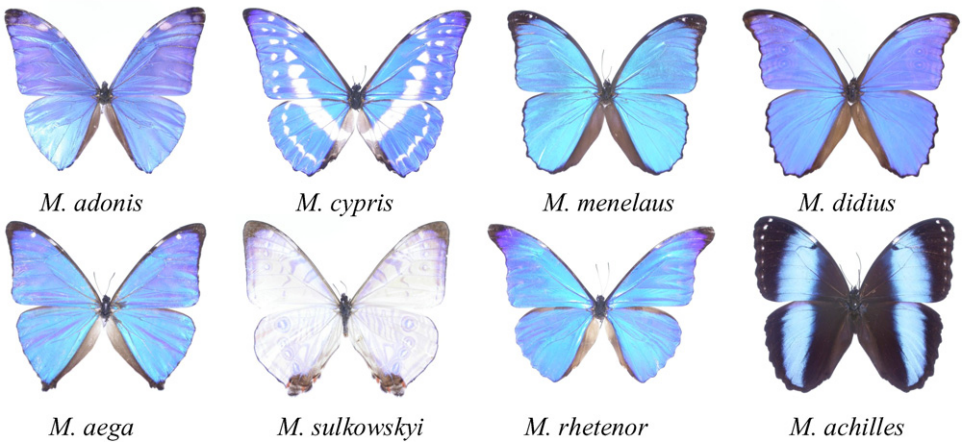

Figure 8. Typical male *Morpho* butterflies (Courtesy of The Museum of Nature and Human Activities, Hyogo, Japan).

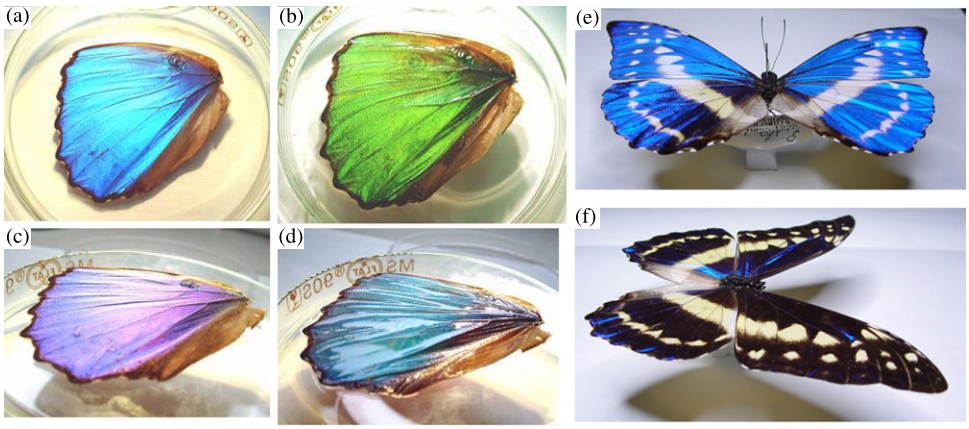

Figure 9. Frontal and oblique views of the *Morpho didius* wing (*a*) and (*c*) in air and (*b*) and (*d*) when immersed into liquid ethanol. Color change of the *Morpho cypris* wing observed when the viewing angles are changed, keeping the direction (*e*) perpendicular and (*f*) parallel to the wing veins.

the most representative animals possessing structural color. The *Morpho* butterflies, shown in figure 8, inhabit South and Central America, and according to the recent classification [39], they are classified into the family Nymphalidae, which consists of several subfamilies including Morphinae closely related to the subfamily Satyrinae. The Morphinae is classified further into three tribes, to which the tribe Morphini belongs. Thus the so-called *Morpho* butterflies are those belonging to a genus *Morpho* in the tribe Morphini, and several tens of species are now known to exist (see figure 8).

In most of the male *Morpho* species, the dorsal wings display brilliantly blue, but their ventral side is usually dark brown, which reminds us of the satyr butterfly. The female is generally less shining or completely non-shining. Thus, there are usually three biological explanations for the blue coloring in the male. One is that the shining blue is for a mating purpose against a resting female. Another is to make predator birds feel dizzy by giving a strong blinking flash. The third is for territorial purposes against other males, because a piece of blue metallic paper is known to attract male *Morpho* butterflies.

Before proceeding in detail, we show the most remarkable features of the *Morpho* butterfly through simple experiments. (1) The first one is the viewing-angle dependence of the wing color. When one sees a specimen of the *Morpho* butterfly from above, one actually perceives strong blue coloring. But, when the viewing angle is inclined obliquely while maintaining the direction perpendicular to the wing veins, one notices that the color does not change at first, but when the angle becomes large enough, the wing color changes into violet or dark blue rather suddenly. In contrast, if one sees the wing keeping the direction parallel to the wing veins, the blue color abruptly vanishes and the wing turns black (see figures 9(*e*) and (*f*)). The degree of color changing is dependent on the species. For example, in *Morpho cypris*, the wing color changes very quickly into black, while in *M. didius*, its change is rather dull. Thus one can easily understand the peculiar feature of structural color in this butterfly; blue coloring in a wide angular range with an abrupt change into violet at large viewing angles, and the anisotropic reflection dependent on the viewing direction. All these observations are quite in contrast to ordinary iridescent animals and manufactured goods.

(2) The second experiment is carried out by immersing the wing into a liquid. Let us use alcohol as a trial liquid. Surprisingly, its color changes to green with slightly dull shining and the oblique view shows blue instead of violet (see figures 9(*a*)–(*d*)). The use of water is inappropriate, because it does not soak into the wing. The change in color is dependent on the refractive index of the liquid employed. Ethanol has

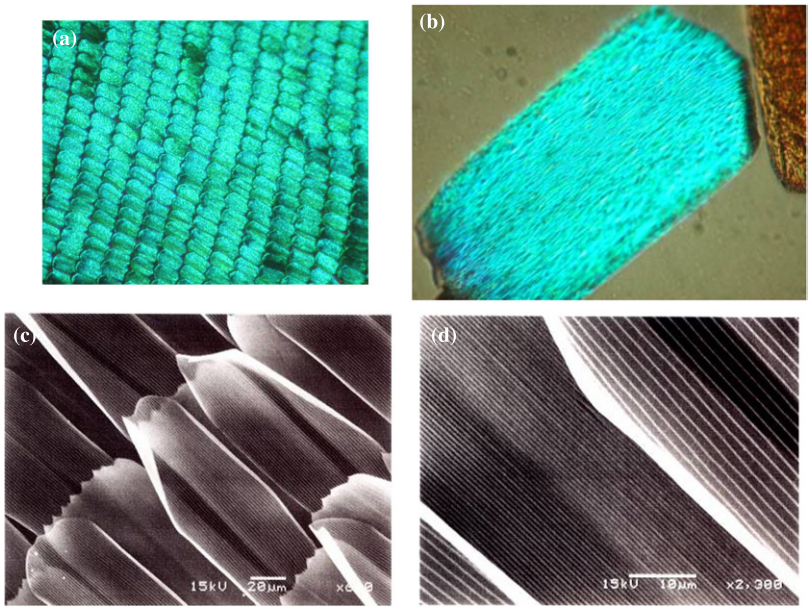

Figure 10. Optical microscopic images of (*a*) dorsal wing and (*b*) scale of *M. rhetenor* observed under epi- and transmitted illumination. (*c*) and (*d*) Scanning electron microscopic images of the scales of *M. didius* [6]

a refractive index of 1.359. If we employ a liquid with a much higher refractive index such as toluene of 1.497, then the following happens: the wing changes to dark brown with no shining. These changes in color restore quickly when the liquid is evaporated. Thus, the change in the color by adding liquid is another typical feature.

(3) The third experiment is to observe the wing using a stereomicroscope. Under a microscope, we can see regular rows of thin plates, as shown in figure 10(*a*). These plates are so-called scales, which are shining blue when the wing is illuminated from the upper side. The blue shining is quite sensitive to the direction of illumination. It is shining only when the wing is illuminated from the direction perpendicular to the long axis of the scale. This experiment is further evidence for the anisotropic reflection described above. If the scale is not flat but is curved such as in *M. achilles*, the dependence on the illumination direction is more peculiar. The shining area looks like connecting lines on the scales and its position is changeable with the direction of illumination.

Let us observe a scale itself by removing it from the wing. One notices that various forms of scales are present depending on the species and the position of the wing. In the blue iridescent region of the wing, two types of scales are usually present. One is called *cover scales* (glass scales), below which the other type of scale called *ground scales* (basal scales) are present (see figure 10). The ground scale usually takes the form of a rectangular shape, whose typical size is 0.2 mm in length and 0.1 mm in width. The cover and ground scales are attached to the wing membrane alternately through holes called a *socket*.

On the other hand, the shapes of the cover scales vary from species to species. In *M. adonis*, a cover scale is large and round: in *M. didius*, the size is nearly the same as the ground scale and its shape is rectangular. In *M. sulkowskyi*, it is slender, and in *M. aega*, the length is less than a half of the ground scale. In *M. rhetenor* and *M. cypris*, a very small cover scale is present at the root of the ground scale. If we employ the transmitted illumination, the cover scale usually looks transparent, while the ground scale looks dark brown. Thus the presence of the pigment is easily confirmed. In *M. sulkowskyi*, both cover and ground scales are nearly transparent, which makes the wing of this butterfly whitish. With further magnification, one can see that a scale has a lot of lines running along the longer side of the scale as shown in figures 10(*b*)–(*d*). These lines are called *ridges* (or *vanes*) and become the most important part of the blue coloring.

(4) Finally, it is instructive to observe the reflection pattern from the *Morpho* wing under the illumination of white or blue light. One can see a long and narrow blue band extending perpendicular to the wing veins. The degree of the slenderness depends on the species: in *M. rhetenor*, it is very slender, while in *M. didius*, it is rather oval. It is remarkable that the reflection pattern is extremely different from a diffraction grating, the latter of which should show diffraction spots. It will be soon understood that the mechanism not to make diffraction spots is quite important for this butterfly, because the butterfly should be perceived from any direction.

Thus, these simple experiments have already revealed the most important part of the structural color in this butterfly. We show how and why the above-mentioned characteristics come out in such a tiny scale on the wing.

4.2. History of Morpho studies

In 1895, Walter (see [9]) reported the color changes of the *M. menelaus* wing immersed into various liquids. Michelson [10] reported that the wing of *M. aega* resembled the surface reflection from a very thin surface layer involving dyes of less than 100 nm thickness. Onslow [12] investigated three *Morpho* butterflies and considered that the surface layer consisting of

chitin plates, acting as a grating and diffraction/interference was a major cause of the color. Süffert [40] reported the angular dependence of reflection color for *M. aega* and *M. achilles*, and considered that the interference was the major cause of the shining. Mason [17] described that in *M. menelaus* and *M. sulkowskyi*, two types of scale covered the wing, both of which had straight *vanes* separated by about 1 μm with a height of 2–3 μm. The vanes in the outer scale (cover scale) were sparsely distributed with a separation of 1.5–2.0 μm and the iridescent blue was observed even in a vane separated from a scale. The inner scale was equipped with very dense vanes and was pigmented. He described the iridescence of these butterflies as coming from the lamellar structure in an individual vane.

Electron microscopic studies of the *Morpho* butterfly were performed independently by Anderson and Richards [20], and by Gentil [21]. Anderson and Richards investigated the wing of *M. cypris* and found hundreds of vanes possessing linear thickenings 0.125 μm apart on the scale. They deduced that the diffuse and multicolored reflection was due to variations in their interval and thickness. Gentil investigated the scales of three *Morpho* butterflies, and found that a wavy lamellar structure observed in each vane was responsible for the iridescence. Later, Lippert and Gentil [41] reported a much sharper microscopic image to show the cross section of an iridescent scale and found a definite lamellar structure in each vane, which consisted of cuticle and air. Ghiradella [42] reported microscopic images for ground scales of several *Morpho* species. She examined various lepidopteran scales and classified the iridescent scales morphologically into (1) laminar thin film, (2) diffraction lattice, (3) Tyndall blue, (4) microrib-satin, (5) microrib thin film, and (6) lamellar thin film, taking account of their mechanisms. She categorized the *Morpho*-type scale into (6) [43–45].

In contrast to the structural and biological progress, the optical and/or physical approach to the iridescence of the *Morpho* wing was somewhat off the pace. Wright [46] measured the angular dependence of the reflected light from the wing and found that the reflection was not caused by simple multilayer interference due to the lamellar structure nor simple diffraction due to the regular rows of vanes. Pillai [47] also reported the angular and wavelength dependence of the reflection from the *Morpho* wing, and deduced that the multilayer interference and diffraction phenomena were interconnected complicatedly. Thereafter, no physical approach appeared until the 1990s and the *Morpho* coloring was considered to be solely due to multilayer interference based on alternate layers of cuticle and air.

Since the 1990s, the scientific research on *Morpho* butterflies has progressed rapidly, and various elaborate measurements and sophisticated calculations have been performed [48–66]. This is partly because structural color attracts great attention in a wide variety of industrial research particularly in painting, automobile, cosmetics and textile industries, because its color is gentle to the eye and also to the environment while possessing strong stimulus to human perception.

With this tide, Tabata *et al* [50] investigated quantitatively the wings of *M. adonis* and *M. sulkowskyi* by optical measurements using an angle- and wavelength-resolved reflection spectrometer. The measurement of the transmission and reflection properties of a single scale was for the first time performed by Vukusic *et al* [53]. The significance of the single-scale measurement lies in the fact that the measurement on the large wing area suffers from various effects due to the scale alignment and from extraneous effects due to non-iridescent scales and the wing membrane. They chose a ground scale of *M. rhetenor*, and a cover and ground scale of *M. didius* as samples, and found that the reflection from a *M. rhetenor* ground scale appeared as two distinct lobes, while that from *M. didius* cover and ground scales showed broad lobing. They attributed this to the distribution of the tilt angle of ridges. In the transmission side, clear diffraction spots corresponding to the spacing of the ridges were found. They measured the absolute reflectivity and found 70% at 450 nm for *M. rhetenor*, while 5–10% and 40% for cover and ground scales of *M. didius*, respectively. They analyzed the high reflectivity of the *Morpho* scale using the multilayer interference model. By fitting to the experimental data, the refractive index of $1.56 + 0.056i$ at 450 nm for a ground scale of *M. rhetenor* with the Gaussian distribution of the ridge tilt of $\pm 15^\circ$ was obtained. Recently, Berthier *et al* [64] reported the optical measurement on the wings of totally 14 species of the genus *Morpho* and classified them according to the size of the cover scale, the tilt angle of the shelf, the lamellar number and the bidirectional reflectance distribution pattern obtained by scanning the direction of detection hemispherically over a wing. They found a photonic-crystal type periodic structure consisting of shelves within one and adjacent ridges, and vertical trabeculae between shelves.

On the other hand, our group paid special attention to irregular structures inherent to natural products and noticed that the interplay between regular structure within a ridge and irregularity among ridges was extremely important for understanding the strongly blue and yet remarkably diffusive nature of the *Morpho* wing [56, 57, 59, 61, 62]. We proposed a simple model to explain the essential part of the *Morpho* coloring and its validity was confirmed by fabricating the *Morpho* substrates, which only mimicked the principle of the *Morpho* coloring [67, 68]. It was shown that the largely anisotropic character of the reflection from the wing was due to a slender shape of the shelf on the ridge, which was interestingly modified by placing wavelength-selective, anisotropic light-diffusing scales on the iridescent ground scales [59]. Moreover, it was clarified that the role of melanin pigment in the structurally colored wing was to enhance the blue coloring on the one hand, while on the other hand, it was to show the wing whitish using special structural modifications in addition to the removal of the pigment [62]. The details of our work are described in the following section.

Owing to recent computational development, it is possible to calculate directly the electromagnetic field around the microstructure and in the far field. The finite difference time domain (FDTD) algorithm is an effective method to calculate the scattering problem due to complicated structures by evaluating the field amplitudes on space–time grids. Plattner [60] employed this method to extract the scattering feature using four types of model structures, a rectangular lattice with

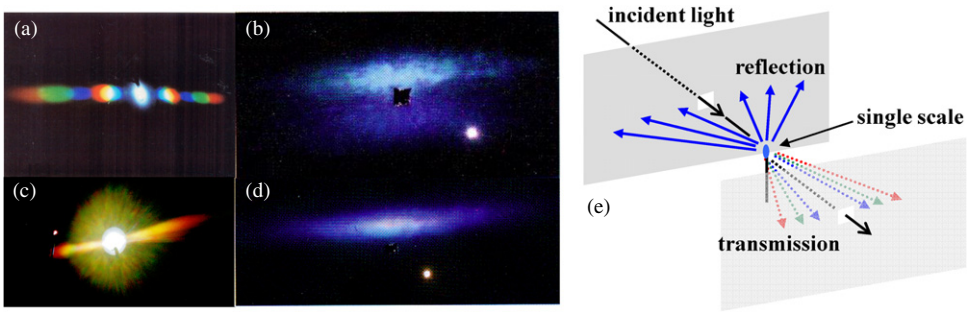

Figure 11. (*a*) and (*c*) Transmission and (*b*) and (*d*) reflection patterns from (*a*) and (*b*) a single cover and (*c*) and (*d*) a ground scale of *M. didius*. (*e*) Experimental arrangement for obtaining the transmission and reflection patterns from a single scale [6].

and without tapering, and an alternate lattice of rectangular elements with and without tapering. He found that a strong extinction of the specular reflection occurs for an alternate lattice and also a tapered model enhances the backscattered power into the first order diffraction spot. Banerjee *et al* [66] employed the algorithm of the non-standard FDTD method to calculate a ridge structure mimicking a *M. sulkowskyi* scale. They employed a refractive index for cuticular material as 1.56+0.06i and calculated the reflection spectrum for unpolarized and polarized incidence, which was in fairly good agreement with the experiment.

These computational methods are actually powerful to solve the complicated scattering problem, because they provide exact results within the framework of Maxwell's electromagnetic theory. However, it is clear that the closer the model approaches an actual structure, the more exact the results should become. Thus in the limit, it is completely equivalent to what we call *measurement*. Therefore it is extremely important to find a proper model, which reduces the complicated structure into an essential part of the phenomenon to search for what is the most important feature for understanding structural color.

4.3. Physical interpretations of the Morpho colorings

4.3.1. Microscopic observations. In this section, we will clarify the mechanism of the structural colors in the *Morpho* butterflies following our recent work [56, 57, 59, 61, 62].

First, we show the results of microscopic observations of the *Morpho* wing. As described above, the scale structures of the *Morpho* butterflies have a wide variety and their physical mechanisms have not been truly clarified except for a few species. Here, we will concentrate on such species whose mechanisms are known at least to some extent. Nevertheless, it is sufficient to show their sophisticated structures and ingenious mechanisms. For this purpose, we have chosen three *Morpho* species, *M. didius*, *M. sulkowskyi* and *M. rhetenor*, as typical examples.

As shown in figure 10(*c*), the dorsal wing surface of the male *M. didius* is covered with two kinds of scales: cover scales of a slender shape and slightly overlapping ground scales of a rectangular shape. The cover and ground scales have a lot of minute ridges with a pitch of ∼1.4 and 0.6–0.7 μm, respectively. The cover scale is transparent, while the ground scale is pigmented so that under transmitted illumination, the latter looks dark brown. The wing of the male *M. sulkowskyi* consists of alternately arranged, transparent ground and cover scales having a normal and slender shape, respectively. The ridge separations of both scales are ∼1.0 μm. Since they lie without much overlapping, it seems that the cover and ground scales essentially have the same structure, and there is no division of role in these scales. The wing of the male *M. rhetenor* consists of overlapping, rectangular ground scales with negligibly small cover scales at their roots. The ridge separations of the ground scales are ∼0.7 μm. The ground scale is pigmented as in *M. didius*. Therefore, the iridescence in *M. rhetenor* is caused solely by ground scales.

In the past, these regularly running ridges were considered to act as a diffraction grating, but the following single-scale experiment clearly defies this expectation. The transmission and reflection patterns obtained for a single cover and ground scale of *M. didius* are shown in figure 11. For the transmission side, diffraction effects can be clearly seen as spectrally separated spots [53, 56]. We can see up to the second order for a cover scale, while only the first order for a ground scale with yellow diffuse scattering around the center. The diffraction angle calculated from this pattern just agrees with that expected from the separation of the ridges. In contrast, and really surprisingly, the reflection pattern does not show any diffraction spots and a broadly extended, blue pattern is observable, which extends perpendicular to the ridge direction. The reflection pattern from a ground scale of *M. rhetenor* is particularly slender. In a cover scale of *M. didius*, a double pattern with slightly different colors is observed [59]. These results are quite unusual in an ordinary sense of optics, because the spacing between ridges actually works as a diffraction grating in the transmission side, while the ridge itself does not in the reflection side. Thus something mysterious is hidden within a ridge.

In order to investigate the structure of the ridge in more detail, we cut a scale and observed the cross section under high magnification. First we show the case of a ground scale of *M. didius*. Obviously, a ridge has a microstructure (figure 12(*a*)), which is more vividly observed in the cross section (figure 12(*c*)). It is clear that a ridge with ∼2 μm height and ∼0.3 μm width has a *shelf structure* like a bookshelf in a library [20, 21, 41, 42]. The vertical separation between the shelves is about 0.2 μm, which reminds us of blue coloring through light interference in a simple multilayer system. As a whole, the shelf structures are not as regular as atoms in

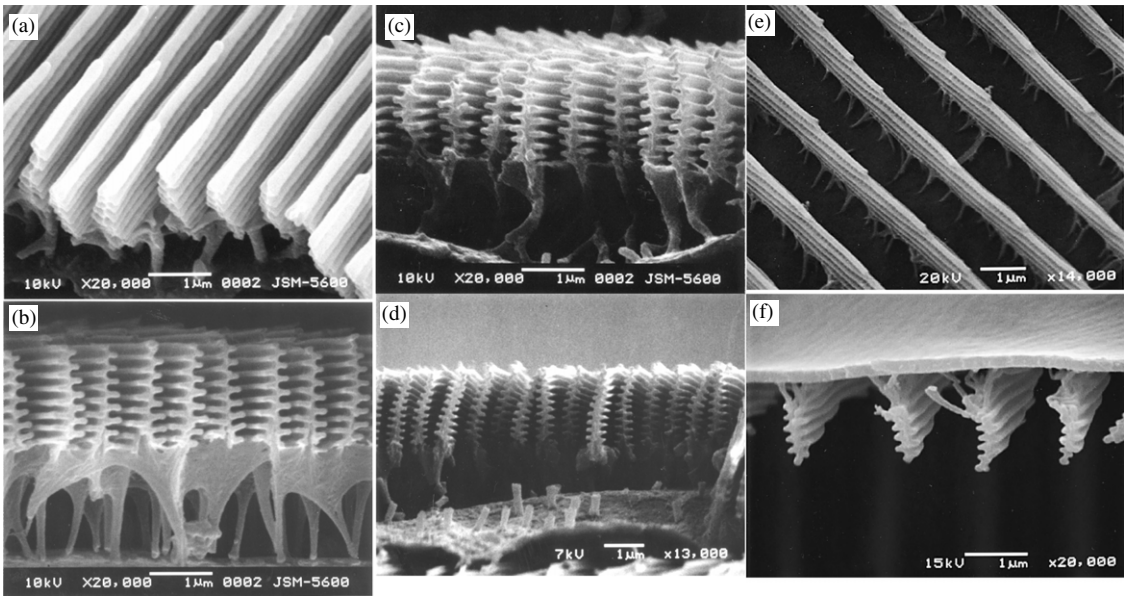

Figure 12. SEM images of (*a*) and (*c*) ground and (*e*) and (*f*) cover scales of *M. didius*, ground scales of (*b*) *M. sulkowskyii* and (*d*) *M. rhetenor* [56, 57, 59]. (*a*)–(*d*) and (*f*) are the cross section of a scale. Note that the photograph (*f*) is upside down.

a crystal, but not as random as particles in a powder. Thus moderate regularity is present as is usually the case in a living system. Close inspection of the cross section shows that a ridge consists of 6–7 shelves of 0.08–0.20 μm in width and 0.05–0.07 μm in thickness and a pillar of 0.05–0.12 μm in width standing at the center. The average thicknesses of the shelf and air layers are approximately 0.055 μm and 0.165 μm, respectively. The directions of the pillar are slightly distributed and only 4–5 shelves near the bottom seem to fully grow. The left and right sides of the shelves seem to stick alternately, but they are not so regular in periodicity and direction. In *M. sulkowskyi* (figure 12(*b*)), the shelf structure is essentially the same as in a ground scale of *M. didius*, although it seems more regular. In a ground scale of *M. rhetenor*, the shelf structure is further developed and more than 10 shelves are discernible (figure 12(*d*)).

Detailed observation reveals that the shelf is not parallel to a base plane, but is oblique to the scale plane with an inclination angle of 7–10° [17, 20, 21, 50, 53]. As shown in figure 12(*a*), the upper ends of the shelves are easily noticed in the image, which are seemingly in a random distribution. If this is true, the height of the ridge will be also distributed when we look at a cross section. The distribution of the ridge height will not be so large and will remain within the separation of the shelves, say 0.2 μm. We have investigated the ridge height distribution and found that spatial correlation between the neighboring ridges was found to be absent [57]. This fact is extremely important to understand the cause of the blue coloring truly, because the random height distribution eventually cancels the interference between the neighboring ridges, and then produces the diffusive reflection as if each ridge scatters light independently.

Next we investigate a cover scale of *M. didius* [59]. As shown in figure 12(*e*), the ridges in the cover scale are distributed regularly but seem to be rather sparse. The shelf structure is similar to the ground scale (figure 12(*f*)), but seems not to grow well. The shelves are also running obliquely to the base plane. However, the characteristics of the cover scale are such that the ridges are attached directly to a thin base plate of thickness 190–230 nm, which is in contrast to the case of a ground scale, where the ridges are built on the complicated trabeculae. At a glance, the ground scale is mainly responsible for the structural color in *M. didius* and the transparent cover scale affects the structural coloration little. However, as described later, the cover scale plays an important role in the wing appearance and even in the reflectivity of the iridescent wing.

4.3.2. Optical measurements. Next, we show the optical properties of the wings of the above three species quantitatively. First, we show the reflection and transmission spectra of the wings. Since both the reflection and the transmission patterns are extended in angle, we have to use a spectrophotometer equipped with an integrating sphere. Since the optical response of matter should be generally expressed by the sum of transmission, reflection and absorption of light, we have divided the optical response of the wing into the above three parts.

The result is shown in figure 13. The transmittances of the wings of *M. didius* and *M. rhetenor* are very low below 500 nm and increase towards the near-infrared region, while that of *M. sulkowskyi* shows extraordinarily high values especially above 500 nm. As a result, the absorption is especially small for *M. sulkowskyi*, while the other two occupy a large part of the visible region of 300–700 nm. Thus the whitish color of *M. sulkowskyi* comes primarily from the lack of pigment in the wing. However, we should not be hasty in drawing this conclusion, because what we perceive is not the absorption but the reflection from the wing. It is rather strange that *M. sulkowskyi* shows an extraordinarily high reflectivity up to 70% at around 460 nm, which is much larger than those of 55%

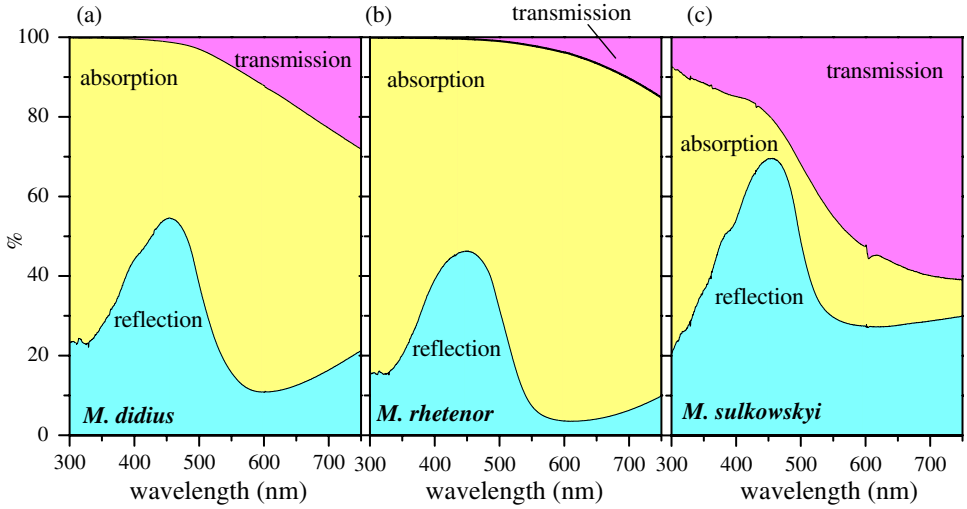

Figure 13. Transmittance and reflectivity in a wavelength range 300–750 nm for the wings of (*a*) *M. didius*, (*b*) *M. rhetenor* and (*c*) *M. sulkowskyi*. The remainder is assigned as absorption [57].

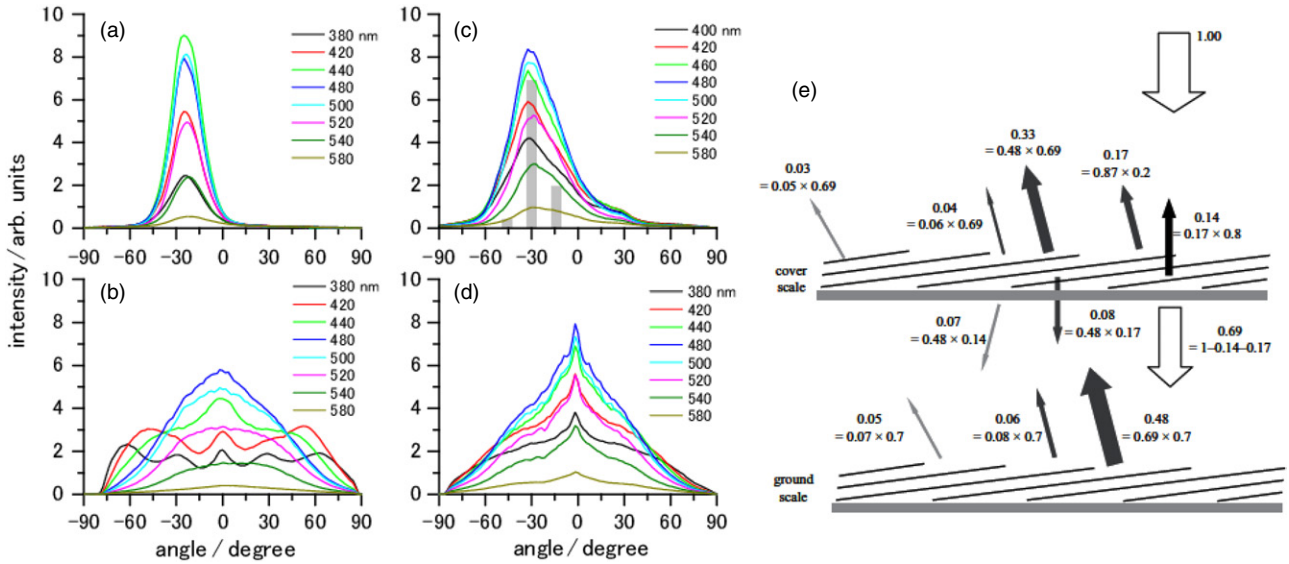

Figure 14. Angular dependence of the reflected light intensity from a dorsal wing of *M. didius* under monochromatic illumination between 380 and 580 nm. (*a*) and (*c*) are obtained under normal incidence and measured within a plane parallel to the ridge for the wing without and with cover scales, respectively. (*b*) and (*d*) are those measured within a plane perpendicular to the ridge for the wing without and with cover scales. (*e*) The cooperative function of cover and ground scales divides the reflection directions roughly into three, indicated as a histogram shown in (*c*) [59].

and 45% for *M. didius* and *M. rhetenor*, respectively. It is noticeable that the strongly blue-reflecting *M. rhetenor* shows the lowest reflectivity.

In reality, the most important point is the reflectivity at a complimentary color at 560 nm rather than the maximum reflectivity at 460 nm. The strongly blue-reflecting *M. rhetenor* hardly reflects the light in a complimentary color region. In fact, it reflects the light only by 3–4%, while the slightly dull-blue wing of *M. didius* shows 10% reflection and the whitish *M. sulkowskyi* amounts to 27%. The high reflectivity at 460 nm of *M. sulkowskyi* seems to be due mostly to the high background reflectivity. Considering this, we deduce that the net reflectivity due to the shelf structure reaches essentially the similar value of ∼40%: 43% for *M. sulkowskyi*, 45% for *M. didius* and 42% for *M. rhetenor*. Thus, *M. sulkowskyi* adds white background to blue structural color to adjust the saturation of the blue color.

Next, we show the angular dependence of the reflected light intensity from the wing of *M. didius* for various exciting wavelengths. The results are shown in figure 14(*d*). It is immediately noticed that the reflected light under normal incidence is widely distributed, regardless of wavelength, and shows a sharp peak in the normal direction. It is also noticed that toward shorter wavelengths, the angular dependence has small shoulders at ±40–60° and for the wavelength shorter than 420 nm, the reflection at large angles is somewhat more intense than that at longer wavelengths, which supports the observation described above.

Since the wing of *M. didius* is covered with two types of scales, we have investigated the roles of these different

types of scale through the angular reflectivity. For this purpose, we remove the cover scales using adhesive tape and measure the angular dependence of reflectivity for the wing covered only with ground scales. It is surprising that the angular dependence in a plane perpendicular to the ridges (figure 14(*b*)) differs considerably from that covered with cover scales (figure 14(*d*)). Namely, the angular dependence is rather widely distributed and the difference in wavelength becomes conspicuous. It shows a maximum at around the normal direction for longer wavelengths, while it shows a peak at around 60° for shorter wavelengths. It is also noticed that the oscillatory structure is observed in the angular dependence and is particularly prominent at shorter wavelengths. Further, a peak observed at the angle of incidence becomes broad and less conspicuous at longer wavelengths.

The angular dependence of the reflection parallel to the ridge is confined within a small angular range (figures 14(*a*) and (*c*)). Actually, the center of the reflection is inclined from the normal to the wing, which was due to that of the scale with respect to the wing membrane and also of the obliquely running shelves [17, 20, 21, 50, 53]. The difference in the angular reflectivity for the directions perpendicular and parallel to the ridges originates from the diffraction effect due to the unidirectional growth of the ridge. Namely, for the direction perpendicular to the ridge, the angular broadening due to diffraction is roughly determined by the width of the shelf of ∼0.3 μm. On the other hand, for that parallel to the ridge, the diffraction is determined mainly by the exposed portion of the shelf with the length of ∼2 μm. If we compare the angular dependence parallel to the ridge, for the wing with and without cover scales, the former is clearly distributed (20°) and asymmetric (figure 14(*c*)), while the latter is symmetric and is confined within a small angular range of ∼10° (figure 14(*a*)). The asymmetric broadening along the ridge is well explained by the cooperative function of the cover and ground scales [59] (see figure 14(*e*)), whereas the angular narrowing perpendicular to the ridge is not clarified yet. Thus, the cover scales in *M. didius* may have the function of reducing the anisotropy of the reflection.

4.3.3. A simple model based on light diffraction and interference. In the following, we will show a simple model proposed recently to explain the essential part of the optical properties in the *Morpho* wing [56, 57, 61]. Although more sophisticated calculations using a FDTD method [60, 66] and a photonic band calculation have appeared recently, these works mostly pay attention to the regular part of the microstructure, and little attention has been paid to the irregular part, which is extremely important in producing the diffusive nature of light.

Here we model the scale structure by considering a system consisting of many ridges, each having several shelves. The height of the ridge is distributed in a random manner within the range of shelf separation. Under this condition, we consider a model to explain the diffraction/interference effect in these structures. To extract the essential part of the regular shelf structure, we have assumed that each shelf has an infinitesimal thickness. This assumption eliminates complex boundary conditions at each surface of the shelf, the refraction inside the shelf and also the intensity reduction of the incident and reflected light at the other shelves. Instead, it neglects the multiple reflections within the shelves and with neighboring ridges, which may weaken the interference effect and neglects the effect of coherent back scattering. However, owing to the narrow width of the shelf, the interference effect due to multiple reflections within a ridge is considered to be not so large. We assume that each shelf has a width a and the shelf separation is taken so as to agree with the optical path length calculated for an actual shelf structure. Thus, in our model, regularly arranged shelves produce quasi-multilayer interference, and the $0.3 \times 2\,\mu\mathrm{m}^2$ size of the shelf contributes to anisotropic light diffraction. Furthermore, the random height distribution gives an incoherent effect among ridges.

Consider first the case that a single shelf is located at a position whose center is expressed by a 2D Cartesian coordinate (x, y). The shelf is assumed to be placed parallel to the x-axis. Incident light illuminates the shelf from the direction of θ and diffracted light is emitted toward the direction of ϕ. The phase difference between the light incident on the origin and the center of the shelf is expressed as

$$k\{x(\sin\theta + \sin\phi) - y(\cos\theta + \cos\phi)\} = k(xu - yv), \qquad (16)$$

where $k = 2\pi/\lambda$ with the wavelength of light λ, and $u \equiv \sin\theta + \sin\phi$ and $v \equiv \cos\theta + \cos\phi$. If M shelves are arranged periodically along the y-axis and N such shelf structures stand equidistantly with a pitch of b along the x direction, then the electric field in the far field is calculated as

$$E \propto \sum_{n=0}^{N-1}\sum_{m=0}^{M-1}\int_{x_n-a/2}^{x_n+a/2} \mathrm{d}x' \mathrm{e}^{\mathrm{i}k(x'u - y_{nm}v)} E_0 \cos\theta, \qquad (17)$$

where we put $x_n = nb$ and $y_{nm} = y_n - md$ with y_n the deviation of the height of the nth ridge from the average, and E_0 the electric field of incident light. The calculation of equation (17) results in

$$E \propto \frac{\sin(kdvM/2)}{\sin(kdv/2)}\frac{a\sin(kua/2)}{kua/2} \times \sum_{n=0}^{N-1} \mathrm{e}^{\mathrm{i}k(nbu - y_n v) + \mathrm{i}kdv(M-1)/2} E_0 \cos\theta. \qquad (18)$$

Then the cycle-averaged intensity of diffracted light becomes

$$I_\phi = \frac{1}{2}|E|^2 = \frac{a^2}{2}\cdot\frac{\sin^2(kdvM/2)}{\sin^2(kdv/2)}\cdot\frac{\sin^2(kau/2)}{(kau/2)^2} \cdot F_R \cdot I_0\cos^2\theta, \qquad (19)$$

with $F_R = |\sum_{n=0}^{N-1}\exp[\mathrm{i}(kbun - \psi_n)]|^2$. The factor ψ_n is the phase difference at the nth ridge due to the height distribution of the ridge and is expressed as $\psi_n = ky_n v$. Here, the terms $\sin^2(kdvM/2)/\sin^2(kdv/2)$, $\sin^2(kau/2)/(kau/2)^2$, and F_R express the interference within a ridge, the diffraction by a single shelf and the interference between different ridges, respectively. If there is no spatial correlation among ridge heights, then the factor F_R reduces to

$$F_R = N\langle|\exp[\mathrm{i}(kbun - \psi_n)]|^2\rangle = N, \qquad (20)$$

and any interference term between different ridges disappears, where $\langle\cdots\rangle$ denotes the ensemble average. This means that the

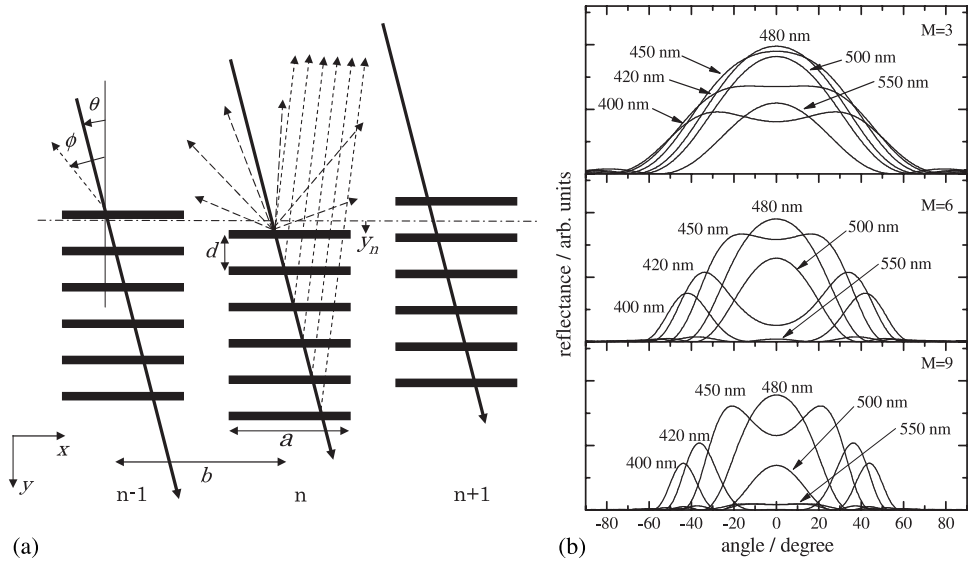

Figure 15. (*a*) A model to calculate the diffraction/reflection properties of the shelf structure on a scale. (*b*) Angular dependence of the reflectivity calculated under the assumption that a plane-wave incident on 3, 6 and 9 layers of 300 nm in length and 235 nm interval is diffracted at each layer under normal incidence [57].

diffracted light emanating from each ridge does not interfere coherently, and that the wavelength and angular dependence of the light reflected and diffracted from a scale can be considered to originate essentially from the shelf structure within a ridge. Thus the total diffraction results from the incoherent sum of single-ridge diffraction. On the other hand, if spatial correlation exists among the ridges, the coherent effect will modify the reflection pattern, as was reported previously [57].

The effect of the alternately sticking shelf observed in an actual scale is taken into account by considering each contribution of the left and right shelves separately, which is given as

$$I_\phi = \frac{a^2}{2} \cdot \frac{\sin^2(kdvM/2)}{\sin^2(kdv/2)} \cdot \frac{\sin^2(kau/4)}{(kau/4)^2} \times \cos^2\{k(ua + 2v\Delta y)/4\} \cdot F_R \cdot I_0 \cos^2\theta, \quad (21)$$

where Δy is the height difference of the left and right shelves. The expression differs from that of the ordinary shelf structure by the presence of the factor $\cos^2\{k(ua + 2v\Delta y)/4\}$ and also by the diffraction due to the shelf of a half size.

In figure 15(*b*), we show typical examples for the angular dependence of the reflection from the shelf structure sticking symmetrically at both sides of a pillar. The reflectivity has a peak around 480 nm in the normal direction, while at shorter wavelengths, the peaks appear at large angles. The calculated result for six shelves seems to reproduce well the experimental result of *M. didius* without cover scales (figure 14(*c*)). From the calculation, we can deduce the essential features of the *Morpho* butterfly. First, the extensive broadening in the reflection angle comes mainly from the diffraction effect due to the narrow width of the shelf. Second, it is also noticeable that the difference in the angular dependence of the reflection is clearly observed between shorter and longer wavelengths. Namely, at shorter wavelengths, the reflectivity at large reflection angles becomes large, while at longer wavelengths, the reflectivity is maximum in the normal direction with a simple reduction of the reflectivity. This is because at shorter wavelengths, constructive interference occurs at larger reflection angles, while destructive interference occurs in the normal direction. On the other hand, no such peculiar interference effect is observed at longer wavelengths.

This calculation clearly reproduces the peculiar appearance of the *Morpho* butterfly that the color of the *Morpho* wing does not alter significantly when the viewing angle is changed, while the violet color is seen when the viewing direction becomes almost parallel to the wing plane. Thus the color change of the *Morpho* wing originates mainly from the interference/diffraction effect due to the coexistence of the periodic shelf structure and the narrow shelf.

The present model reproduces the angular dependence of the reflection fairly well, which can never be explained using a simple multilayer interference model. The neglect of multiple reflection within a ridge offers a surprisingly good result. This is partly due to the strong diffraction effect as described above and partly due to the irregularity in the actual shelf structure. The change in the color when immersed into liquid is also explained as due to the change in the optical path length between shelves and also to the difference in the refractive indices between the shelf and the surrounding medium.

However, the above model fails to explain the peculiar features such as a peak at the angle of incidence and the oscillatory structure found at shorter wavelengths. It is also noticed that the angular range is limited within $\pm 60^\circ$ in the calculation, while it extends over $\pm 80^\circ$ in the actual wing. We propose two possible mechanisms for the former characteristics by introducing the effect of spatial correlation and the coherent backscattering of light [57]. The angular broadening, on the other hand, owes most to the effect of the alternately sticking shelf structure and also the distribution of tilt angles of ridges [53]. Anyway, the addition of these extra effects will considerably improve the angular dependence in this model.

4.3.4. Effect of pigment. As described above, the major difference between the blue species *M. didius* and the whitish species *M. sulkowskyi* comes from the amount of background scattering above 530 nm as shown in figure 13. To investigate the origin of background scattering quantitatively, we have performed an experiment on *M. cypris* [62], whose fore and hind wings have a distinctive white stripe pattern on the structurally colored blue wing, as shown in figure 8. It is clear from electron microscopic observations that the microscopic shelf structures are essentially the same for the blue and white parts [20, 62], which resemble the ground scale of *M. rhetenor*. Thus the difference in color originates mainly from the presence of pigment. This butterfly aims to show the white spot clearly by removing the pigment largely from the wing membrane and completely from the scales at both the sides.

We have measured the reflection and transmission characteristics of blue and white scales on the dorsal side, brown and white scales on the ventral side, and brown and transparent areas of the wing membrane, and have analyzed the situation using a three-layer model considering the multiple reflection among them. It is found that the background reflection comes almost equally from the dorsal and the ventral scales and a wing membrane, with multiple reflection among them. Among these, a ventral scale shows the usual isotropic scattering, whereas the wing membrane shows specular reflection and the dorsal scale may show a mixture of anisotropic reflection due to the shelf structure and scattering due to the trabeculae. Thus the background scattering has anyway an isotropic character in the scattering direction, which strongly impresses the white color in contrast to extremely anisotropic reflection of the blue color. An additional reason is that the perception in the eyes obeys a logarithmic detection with respect to the light intensity, which strengthens the weak white background and suppresses the strong blue coloring.

Thus, the role of the pigment in the iridescent wing is generally summarized as (1) the enhancement of the blue coloring by adding pigment beneath the iridescent structure to absorb scattered light of complimentary color and (2) the adjustment of color saturation by reducing the pigment without structural change.

4.3.5. Role of cover scale. The shape of the cover scale seems to play a key role in phylogenetic studies [64, 69]. Namely, in ancient groups, the cover scale plays a central role in producing the iridescence or plays an equivalent role to that of the ground scale, but gradually its role decreases with reduction of the size. In the evolved group including *M. rhetenor*, the cover scale degrades almost completely to expose the ground scale directly, while in another group including *M. didius*, the size of the cover scale is large enough to completely cover the ground scale. As a result, in the former, the wings are lustrous, while in the latter, they look frosted blue. Thus the cover scale in the latter group seems to attain a special function to display the wing differently. In order to investigate its role quantitatively, we choose *M. didius* as a sample [59]. The cover scale of *M. didius* has a peculiar structure such that the ridges are sparsely distributed on the base plane (figures 12(*e*) and (*f*)), and its reflection shows a double pattern with slightly different colors, light and deep blue (figure 11(*b*)). Further, the angular dependence for the reflections with and without cover scales are very different (figure 14).

The reflection spectra of deep and light blue-bands are very different: the former has only a single sharp peak around 460 nm, while the latter shows a rather broad peak around 460 nm with increasing reflectivity toward the longer wavelengths. Considering the microscopic structure, we deduce that the deep-blue band comes from the shelf structure in a ridge, while the light-blue band comes from the thin-film interference at the base plane. In fact, the calculation using a thickness of 215 nm with a refractive index of 1.56 gives the second-order interference peak at 447 nm with the maximum reflectivity of 17%, which almost agrees with the experiment. If we assume the total reflectivity as the sum of the two mechanisms, which is determined by the area ratio of 8 : 2 for the base plane to the ridge, the reflectivity amounts to 31%, which is in quite good agreement with the experimental value of 31%. Thus, since the reflectivity of the *M. didius* wing amounts to ≈55%, the cover scale is responsible for more than half of the total reflectivity. The double reflection band originates from the reflection due to a basal plane through thin-film interference, and from that due to obliquely running shelf structure with a gradient of 8°. It is also noticed that the reflection from the basal plane does not show a specular reflection nor diffraction spots, but is distributed like the reflection from a ridge. The reason for this spatial broadening is not clarified yet. Anyway, if such a functional scale is placed on the ground scale of strongly anisotropic reflection, it has the function of extending the reflection angle in the direction of the running ridge (figure 14(*e*)) and thus to weaken the anisotropy of the reflection.

The cover scales of *M. didius* have carefully designed microstructures that function as the selective optical diffuser for blue light. Further, the cooperation of the ground and cover scales makes possible the high reflectivity in a wide range of solid angles. This function may play the role of reducing the gloss of the wing and to show a different appearance due to diffuse angular reflection and broad reflection spectrum.

4.3.6. Reproduction of the Morpho coloring Thus, the cooperation of the regular and irregular structures plays a central role in displaying the blue appearance of the *Morpho* butterflies. In order to confirm this hypothesis, we have fabricated the *Morpho* substrate artificially only by mimicking its principle [6, 67, 68]. First, we prepare a transparent or black glass plate. One surface is polished roughly to produce the irregular surface. Then, the multilayer is coated on this rough surface, which assures the regularity. Thus, in addition to the pigment, the coexistence of regularity and irregularity is introduced. The result is shown in figure 16(*b*). The fabricated substrate looks like a *Morpho* wing, because diffuse blue color is reflected intensely and the color change into violet is clearly observed when one views the substrate obliquely. This is in contrast to the case without roughness, where the blue color is only observable at an angle of specular reflection, otherwise the substrate looks black. Thus, our hypothesis for

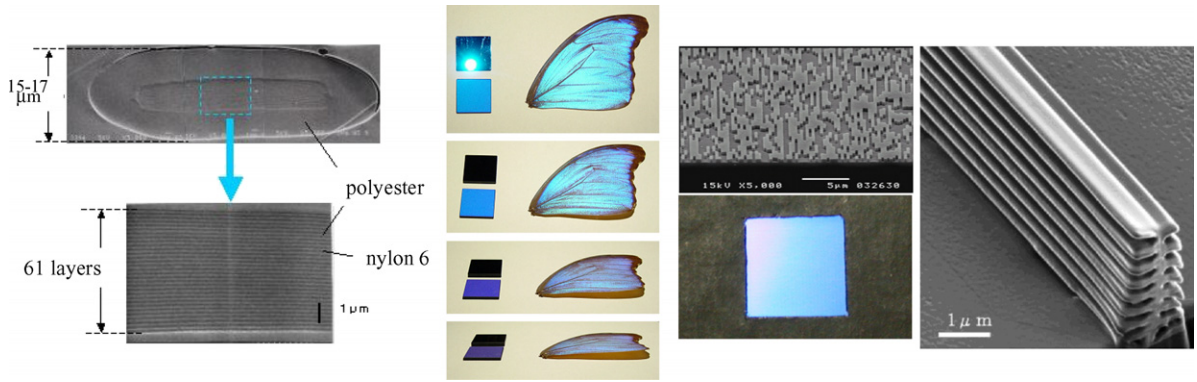

Figure 16. (*a*) Cross section of a fiber mimicking the *Morpho* butterfly (Courtesy of Teijin Fibers Limited). (*b*) Viewing-angle dependence of multilayer-coated substrates with (lower left) and without rough surface (upper left), which are compared with the wing of *M. didius* (reproduced from [67] with permission). (*c*) SEM image of a substrate (before coating) with the random surface structure fabricated by dry etching method and that observed under illumination after multilayer coating (reproduced from [67] with permission). (*d*) Shelf structure fabricated by a focused-ion-beam chemical-vapor-deposition technique (reproduced from [74] with permission).

the mechanism of the *Morpho* blue has been almost confirmed. However, several problems have arisen: the roughness is a key point to the present substrate. If it is too much, multiple scattering occurs and the substrate becomes whitish. If it is too small, specular reflection occurs. Further anisotropic reflection cannot be introduced in the present method. Thus, controlled randomness is anyway necessary.

Then we employ the method of nanotechnology to create the controlled randomness [67, 68]. Dry etching on a quartz substrate is employed to make controlled roughness. We consider a unit rectangle, whose average size is 2 μm in length and 0.3 μm in width, which is the same as the shelf structure on a ridge of a *Morpho* scale. This unit is randomly distributed on the substrate taking two values for the height with the difference in the heights set at 0.11 μm, which is to cancel the specular reflection at 440 nm under normal incidence. Then, multilayer coating with SiO_2 and Ta_2O_5 layers is performed. The fabricated substrate is shown in figure 16(*c*). The upper photograph shows a SEM image of the substrate before coating and the lower one shows a photograph of the substrate whose size is $6 \times 6\,\mathrm{mm}^2$. The anisotropic reflection pattern almost completely agrees with that of a *Morpho* wing. It is suggested that in order to reproduce the *Morpho* blue, we need not mimic the structure itself but only its principle.

4.3.7. Summary of Morpho coloring The physical significance of the above results is summarized in figure 17. (1) The structural color originates mainly from light interference within a shelf structure through quasi-multilayer interference. (2) The slender shape of a shelf gives strongly anisotropic reflection. (3) The irregularity in the ridge height destroys the interference among neighboring ridges, which results in the diffuse reflection in a wide angular range. Thus the combined action of interference and diffraction is essential for the structural color in *Morpho* butterflies. (4) High reflectivity is realized owing to the presence of 6–10 shelves in a ridge with a large difference in refractive indices and also to a sufficiently small separation between adjacent ridges. (5) The pigment beneath the iridescent structure absorbs

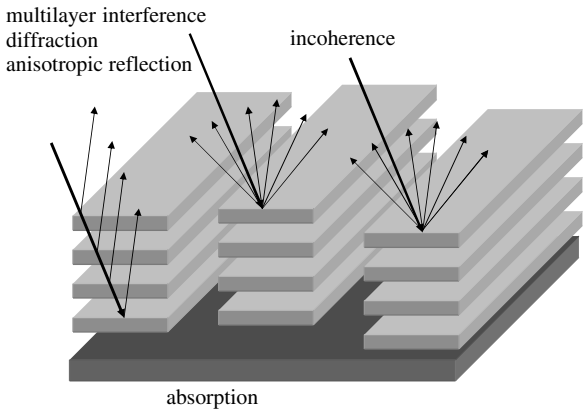

Figure 17. Schematic illustration of essential factors associated with the structural color in *Morpho* butterflies.

the unnecessary complementary color and enhances the blue structural color, while with eliminating pigment, the scattering at the wing membrane and ventral scales adds a whitish color to the wing. (6) Cover scales placed on ground scales give the wavelength-selective optical diffuser to weaken the gloss of the wing. All these effects control the appearance of blue coloring in these butterflies.

4.4. Mimicry of the Morpho butterfly

A new stream of *Morpho* research has quickly developed in this decade. That is to mimic the *Morpho* blue by constructing elaborate structures using recently developed nanotechnology. This work is classified roughly into two categories: one is to mimic the *Morpho* blue coloring and the other is to mimic its microstructure. The former work is related to vision technology, while the latter to photonic technology to search for new photonic devices and their fabrication methods.

In the textile world, a quite sophisticated fiber was invented by Iohara *et al* [70] by mimicking the scale structure of the *Morpho* butterfly. This fiber is made of polyester and has a flattened shape of thickness 15–17 μm, within

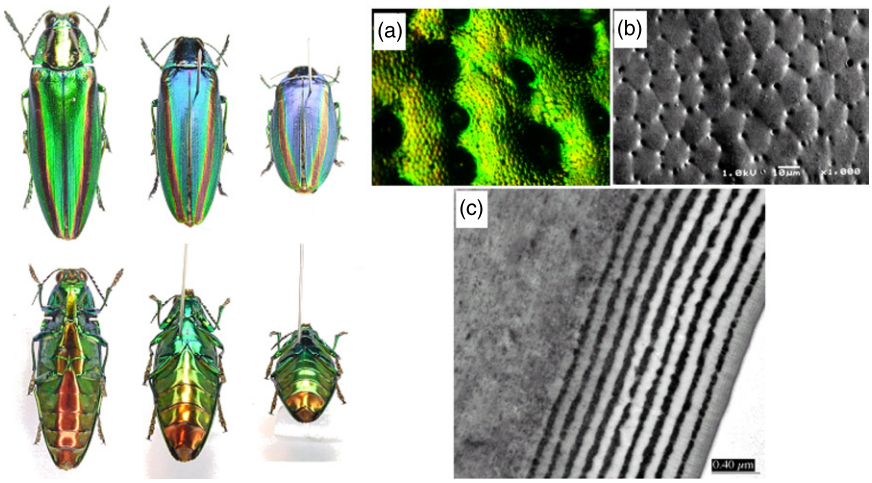

Figure 18. (Left) Viewing-angle dependence of the color change in jewel beetles. (Right) The surface of the elytron is observed by (*a*) optical microscope and (*b*) SEM [6]. (*c*) TEM image of the cross section of the elytron (Courtesy of Professor Hariyama).

which 61 layers of nylon 6 and polyester with a thickness of 70–90 nm are incorporated (figure 16(*a*)). Because of the multilayered structure, wavelength-selective reflection and change with viewing angle are obtained. Moreover, the flat shape of the fiber makes it possible to align the direction of the multilayer, which increases the effective reflectivity. They demonstrated the weaving of a wedding dress using this fiber. Since the polymer materials constituting the layers have similar refractive indices ($n = 1.60$ for nylon 6 and $n = 1.55$ for polyester), the reflection bandwidth is limited within a small wavelength region. In fact, the wedding dress seems to be pale blue and is really in harmony with the ceremony. However, it differs considerably from that of the *Morpho* butterfly concerning the color impact and luster.

Saito *et al* developed our method of fabricating the *Morpho* substrate to be useful for mass production [71]. They employed nanocasting lithography to obtain fine pattern replication using various polymer materials. This method is superior to the conventional nanoimprint lithography, because the former is better for replication without mold damage and the mixing bubbles are easily removed by vacuum baking. The fabricated replica looked very similar to the master plate under scanning microscopic observation and its reflection pattern was found to be similar to the *Morpho* wing. Thus low cost reproduction is attainable, which promises mass production of the *Morpho* substrate.

A completely different approach to mimicking the microstructure of the *Morpho* butterfly itself was developed by Matsui *et al*, who utilized a focused-ion-beam chemical-vapor-deposition technique to reproduce the complete structure of a *Morpho* scale (figure 16(*d*)) [72–75]. This method was based on the following architecture: a Ga^+ ion beam was focused on a sample surface with a small focal size of typically 10 nm, where aromatic hydrocarbon precursor gas was injected through a nozzle located near the sample surface. They used phenanthrene ($C_{14}H_{10}$) as a precursor. The deposited material was found to be mostly amorphous diamond-like carbon, which promised hard and transparent qualities. They adjusted the distance of shelves to agree with that of the *Morpho* butterfly and even to reproduce the alternate shelf structure. The replica illuminated by white light is found to actually glitter blue to violet under microscopic observation.

Thus recent rapidly developing nanotechnology has proved that even the most elaborate structure in nature can be realized. Therefore, the future of the study of structural colors is extremely promising, because the optical and physical investigations on their mechanisms are immediately confirmed by fabricating the structure directly, which enables us to re-investigate the structural and optical properties from first principles.

5. Color-producing microstructures in nature

5.1. Thin-layer interference and its analogue

5.1.1. Jewel beetles. First, we show the most popular and yet most complete biological product of the multilayered system found in beetles (figure 18). The elytra of beetles are usually conspicuous in their brilliant and lustrous reflections, and have been attracting the eyes of people for a long time. In Japan, more than a thousand years ago, the wings of jewel beetles were used to decorate craft work and Buddhist miniature temples.

In contrast to the general attention, the scientific approaches to elucidating the color-producing mechanisms in these beetles are extremely few. In the first half of the 20th century, scientists solely observed the elytra of beetles by giving a mechanical pressure, soaking in a liquid, scraping the surface, and observing the section under an optical microscope [10, 12, 17, 18, 76, 77]. The first electron microscopic observation on this type of beetle was reported by Durrer and Villinger in 1972 [24]. They examined a buprestid beetle, *Euchroma gigantea*, and found that the transverse cross section of the elytron revealed five layers of dark regions regularly arrayed near the surface, below which an irregular fibrous region was located. They deduced that the dark layers were composed of melanin, which was also distributed below the regular layers. The uppermost clear layer had a thickness of 0.2–0.4 μm, which was followed by dark layers of 0.09 μm thickness for the copper brown region of the elytron and

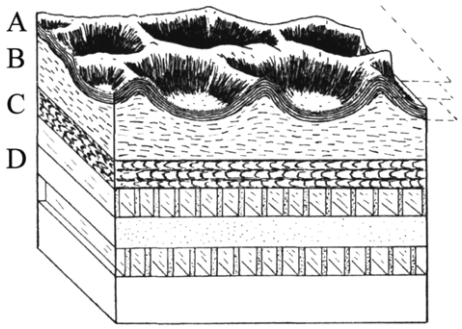

Figure 19. Schematic view of the interior of elytron in tiger beetles (reproduced from [78] with permission). A: strongly alveolated epicuticle with multilayered structure, B: outer exocuticle with dark lamellae, C: inner exocuticule of helicoidal structure and D: endocuticle with plywood structure.

0.06 μm for the green region, while the clear layers between the dark layers were rather constant with 0.06 μm thickness. He also noticed that the arch-shaped modulation at the surface changed the incidence angle to the multilayer system and contributed to various colorings of this beetle.

Complete investigations appeared in 1985 by Schultz and Rankin [31, 78, 79]. They investigated four *Cicindela* species of tiger beetles using optical measurement, chemical treatment and electron microscopic observations. The surface of the elytral cuticle is divided into three regions: epicuticle, exocuticle and endocuticle. They found that the epicuticle region showed a thickness of 1–2 μm and was strongly alveolated with polygonal ridges and hollows with a depth of 3.5 μm (see figure 19). Just beneath the alveoli, 4–9 dark layers were located, which were composed of vertically aligned granules with thicknesses of 0.03–0.1 μm. Between the layers, clear regions with thicknesses of 0.06–0.125 μm were present. Below the epicuticle, an outer exocuticle was present with a thickness of 2–3 μm, which was composed of 25–35 lamellae of 0.055–0.1 μm interval, and constituted an imperfect helicoidal structure. Both epicuticle and outer exocuticle were dark brown and were thought to be melanized. Below it, the inner exocuticle of a peculiar helicoidal pattern and the endocuticle of plywood structure appeared. Similar observations were reported later on leaf beetles [80, 81] and jewel beetles [81].

The characteristics of this type of structural coloration are that the multilayer consists of melanin granules or melanoprotein, which has a severe light absorptive ability over the whole visible region. The incorporation of light absorption into the multilayer system is easily estimated by adding an imaginary part to the refractive index of the layer. In figures 20(*a*) and (*b*), we show such examples for the reflectivity and transmittance for a multilayer possessing absorptive behavior. With increasing imaginary part of the refractive index in one component of the multilayer, the reflectivity naturally decreases with narrowing bandwidth and diffuses the side-lobe structures without much change in the peak wavelength. However, the most remarkable feature is that the transmittance of the background region decreases quickly. This behavior is more easily seen in the total light energy calculated by the sum of the reflected and transmitted light intensity, as shown in figure 20(*c*). With

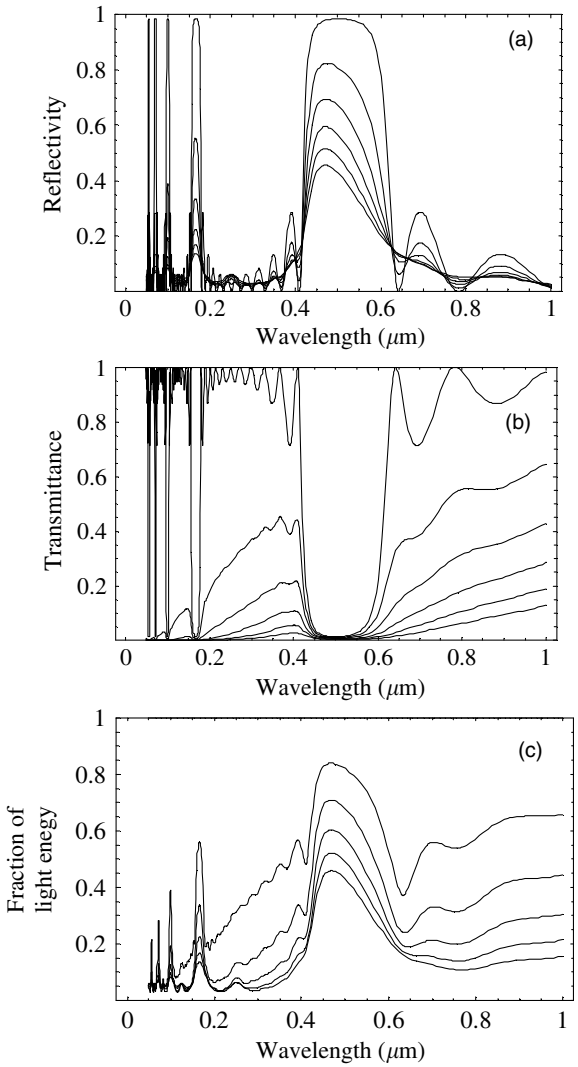

Figure 20. Effect of absorption on the multilayer interference under normal incidence, where 11 alternate layers of widths 78.1 nm and of 125 nm are arranged. The former refractive index is varied as 1.6, 1.6+0.05i, 1.6+0.1i, 1.6+0.15i, 1.6+0.2i and 1.6+0.25i (from top to bottom in (*a*)–(*c*), while the latter is kept constant at 1.0. (*a*) Reflectivity, (*b*) transmittance and (*c*) corresponding light energy calculated from the sum of the transmitted and reflected light intensity. Note that the calculated fraction for 1.6 just agrees with unity in (*c*).

the increasing imaginary part, the fraction of the light energy naturally decreases from unity. It is remarkable that only light energy that belongs to the reflective band tends to remain. Thus the involvement of the absorptive material contributes mainly to background reduction in the multilayer reflection, because the transmitted light more or less contributes to the backscattering of light due to the underlying structures. The background reduction is quite important for iridescent animals to visually emphasize the reflection color by reducing the complimentary color.

Before closing this subsection, we make some comments concerning the optical response. Although the multilayer is probably the simplest system to cause structural color, various problems still remain unsolved: (1) What are the constituents of the dark regions and how can the refractive index be determined

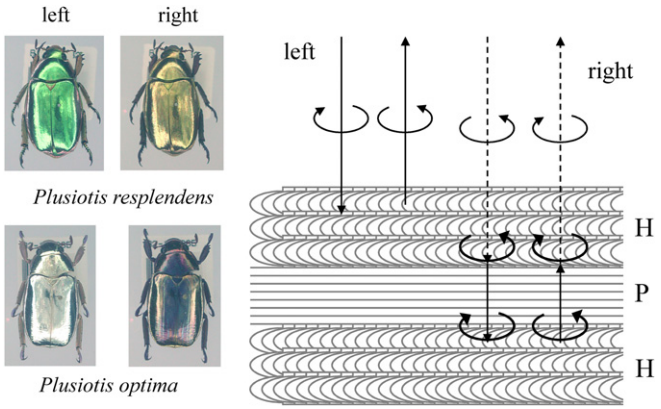

Figure 21. (Left) Scarabaeid beetles observed under circular polarizers (courtesy of The Nature and Human Activities, Hyogo, Japan). *Plusiotis resplendens* shows different colors under left- and right-circular polarizers, while *P. optima* shows silvery color only under left-circular polarization. (Right) Schematic illustration of a sandwiched structure found in *P. resplendens*. H: helicoidal layer, P: unidirectional layer acting as a λ/2 plate

accurately to evaluate the interference phenomenon? (2) How can the effect of surface modifications, like alveoli, on the multilayer interference be properly evaluated? (3) How is the irregularity of the multilayer appropriately evaluated? Hariyama [81] tried to evaluate the density distribution of the dark layer by a densitometer and found a sinusoidal distribution for the electron density rather than the discontinuous layer as has been assumed usually. This finding seems very interesting if we consider the dark layers to be composed of ensembles of melanin granules, which inevitably diffuses the interfacial shape.

5.1.2. Scarabaeid beetles. It was about 100 years ago that a strange parabolic pattern was observed in a section of the cuticle layer in a millipede (see [82]). This pattern was found to be periodically arranged under the cuticle surface of this animal with a total thickness of over 100 μm. Later, similar patterns were reported at the surface layers of crustaceans and insects [82]. Electron microscopic observations revealed that the pattern consisted of many curved lines like scratches scraped by a brush, which were periodically arranged parallel to the surface [83, 84]. The most remarkable feature of this pattern was that it was only observable when the section was cut obliquely. Otherwise, a periodic lamellar structure was observed.

The first analysis of this pattern was performed by Bouligand in 1965 [82], who considered that the pattern came from fibrous elements uniformly arranged in a plane parallel to the surface. Further, the direction of the elements was found to gradually change as a function of the distance from the surface. He noticed that the biological helicoidal structure giving a parabolic pattern was closely related to cholesteric liquid crystals.

Michelson [10] first noticed the anomalous reflection from beetles' elytra. He investigated the reflection properties of the elytron of a golden scarab beetle, *Plusiotis resplendens* (figure 21), and found that the reflected light was circularly polarized even at normal incidence. The degree of the circular polarization was maximum at blue, decreased gradually toward the yellow region, completely depolarized in orange-yellow and reappeared in the opposite direction at the red end. He considered the origin of this circular polarization as being due to a screw structure of molecular dimensions.

This observation was later investigated by Neville and Caveney [23], who reported detailed descriptions of the structural and optical properties in various species of scarabaeid beetles, and found most of the species show circularly polarized reflection. They observed that the colors of the elytra of these species changed with changing viewing angle and a polarizer capable of passing right-circularly polarized light made the elytra completely black (see figure 21). Further, the transmitted light through the excised surface layer showed an optical rotation.

They scraped the cuticle surface minutely and assigned the locations of the unusual optical properties as the outer region of the exocuticle, where a regular lamellar pattern with widths of 4–15 μm and apparent pitches of 153–198 nm was observed. In contrast, the inner region was sclerotized and showed a dark color with an irregular lamellar structure. The lamellar spacing in the outer exocuticle changed systematically to cause reflection in a wide wavelength range. They found that the overall features were very similar to those of a well-known cholesteric liquid crystal. From the investigation of the inner region of the exocuticle of *Anoplognathus viridaeneus*, they found microfibrils spaced about 6.5 nm apart in the direction normal to the cuticle surface. Since the actual helicoidal pitch was found to be $165 \times 2 = 330$ nm from the apparent pitch of 165 nm, the number of layers was estimated at $330/6.5 = 50$ and the rotation angle between adjacent layers was $360^\circ/50 = 7.2^\circ$. The component of the microfibril was clarified as chitin crystallites, which were bound tightly with protein networks [83, 85].

Caveney [86] compared two species of the scarabaeid beetle, *Plusiotis optima* and *P. resplendens* (figure 21). The former appeared silvery, while the latter had a golden luster. The widths of the optically active layers for these beetles were found to be 16 μm and 22 μm, respectively. The layer of the latter species was remarkable because it showed a sandwiched structure, which consisted of a 5 μm thick upper and a 15 μm thick lower layer that showed clear parabolic patterns and a sandwiched layer of 1.81 μm that showed a unidirectional molecular architecture. The reflection spectra for circular polarizations were very peculiar such that for the left-circular one, it showed the peak around the green region of 560 nm, while for the right-circular one, it showed a peak in the orange region around 575–624 nm. Both reflections showed a rather high reflectivity of 0.32–0.35, which amounted to a total reflectivity of 0.6–0.7, while in *P. optima*, only the left-circular light was reflected with a reflectivity of ∼0.5. The reflection of both the directions of circular polarizations and the wavelength shift of the reflection maximum agreed with Michelson's observation [10].

The origin of this peculiar phenomenon was found to come from the presence of the sandwiched layer, which showed optical anisotropy. Caveney [86] calculated the phase change

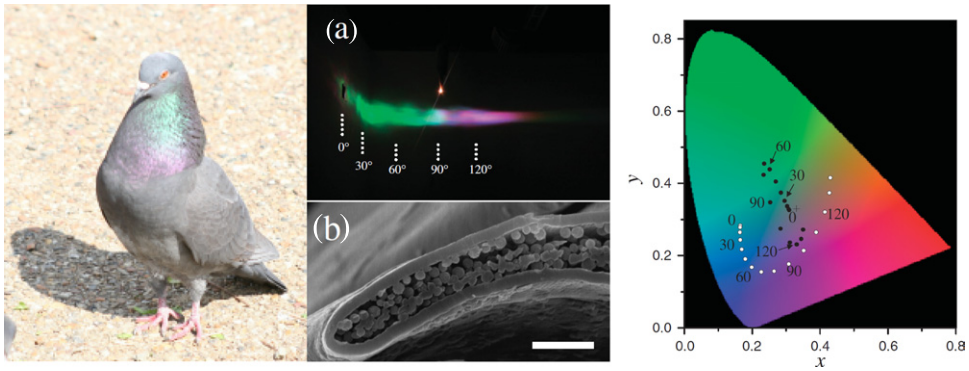

Figure 22. Rock dove, and (*a*) the reflection pattern of a barbule, where 0° indicates the direction of incident white light. (*b*) SEM image of the cross sections of the barbule. The right figure indicates the chromaticity diagram showing the loci of the reflection in thin-layer interference at various angles 2θ for the layer thickness of 650 nm (closed circle) and 400 nm (open circle) with the refractive index of 1.5, where θ is the angle of incidence [33].

due to this layer and found it had a function of a perfect $\lambda/2$ retardation plate around 590 nm, which worked fairly well within a region of 550–650 nm. What happens when a $\lambda/2$ retardation plate is sandwiched between two cholesteric liquid crystals of an anti-clockwise helical system? The answer is as follows (see figure 21): when the unpolarized light is incident normal to the material, the light with left-circular polarization is completely reflected, while that with right-circular polarization penetrates without any loss. The $\lambda/2$ retardation plate changes right-circular light to left-circular light when transmitted. Then the converted left-circular light is selectively reflected in the second cholesteric layer and the reflected light becomes left-circular. The $\lambda/2$ retardation plate again changes the left-circular light to right-circular light, which penetrates the first layer without loss and emerges out. Thus both left- and right-circular light are effectively reflected. It is important that the pitches of the two helicoidal layers are chirped in different ways, which produces the wideband reflection with peculiar circular polarizations.

Caveney [86] measured the refractive indices of these layers and found that they are extraordinarily high in contrast to those of ordinary scarabaeid beetles. He chemically extracted the exocuticle layer and found that a high content of uric acid, volume fraction of 0.6–0.7, was distributed in this layer. Uric acid crystals are known to have a high refractive index of $n = 1.89$ with high birefringence. In order to realize the high anisotropy, strict control of the orientation of the crystals is necessary, which has not been clarified yet.

5.1.3. Rock dove. Next, we show that even the simplest structure of a thin film produces an ingenious color effect to human and possibly animal eyes [32, 33, 87, 88]. In the present subsection, we briefly describe its mechanism through our recent work [33]. The neck feather of the commonly spotted rock dove, *Columba livia*, shows unusual optical characteristics: the green (purple) feather located at the neck, suddenly changes its color into purple (green) only by slightly shifting the viewing angle, which is quite in contrast to the gradual color change observed in usual iridescence. A bird feather consists of a main shaft, from which many barbs branch out. Further, smaller branches called barbules stick out from a barb. The color of the rock dove's feather is mainly due to numerous sticking barbules, whose length, width and thickness are typically 350, 40 and 3 μm, respectively. The cross section of a barbule is crescent-shaped, which produces a very broad reflection pattern in one plane under light illumination. It is remarkable that the reflection pattern from a single barbule of a green (purple) feather shows the sudden change from green (purple) to purple (green) with a rather distinctive gray boundary, as shown in figure 22(*a*).

We have investigated electron microscopic images of the cross section of a barbule and have found that a lot of melanin granules are enclosed within a layer of the outer cortex (figure 22(*b*)). The diameters of the melanin granules are randomly distributed from 500 to 750 nm and their arrangement is also irregular. Thus they may not contribute directly to the coloration. Thus, the cortex layer with a rather constant thickness becomes the one and only candidate for the coloration, whose thickness ranges from 600 to 700 nm for a green feather and from 480 to 580 nm for a purple feather. In fact, the reflection spectra from a single barbule displaying green, gray and purple colors show multiple sinusoidal reflection spectra, which are gradually shifted according to the perceptible color. These spectra are found to be in very good agreement with the expectations of thin-film interference assuming, for example, a layer thickness and refractive index of 650 nm and 1.5 for a green feather.

Thus the coloration of the neck feather of the rock dove is actually caused by the simplest mechanism of thin-film interference. However, optical interference occurs on higher orders, which produce multiple peaks in the visible wavelength range [32,33,87,88], e.g. a green feather shows $m = 3, 4$ and 5 interference peaks at 700, 520 and 420 nm under the incidence angle of 30°. The most important point to produce the *two-color iridescence* is based on the fact that the separation of the two adjacent peaks in wavenumber units coincides with that of the color matching functions of human vision for blue and red. Thus, when this condition is satisfied, one may perceive purple color, while when the viewing angle is changed and hence the reflection peak shifts from red to green and also from blue to ultraviolet, one may perceive only green color. Between these colors, one sees the gray color because all the colors are perceived almost equally.

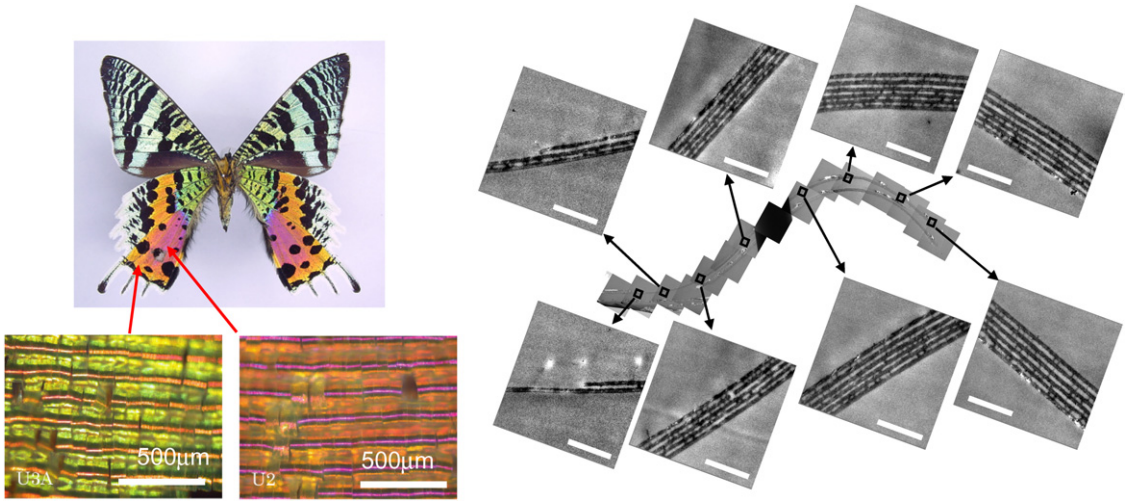

Figure 23. Ventral side of a Madagascan sunset moth, *Chrysiridia rhipheus*, and the optical microscopic images for two regions with different colorings. The right side shows the TEM image of the cross section of a cover scale in the longitudinal direction, where the insets are the enlarged views at various positions [98].

This situation is more clearly understood in terms of a chromaticity diagram, where two-color iridescence is expressed by a linear movement of the loci crossing a white (gray) zone ($x = 1/3$ and $y = 1/3$) as shown in figure 22. It is clear that the multiple peaks due to the thin-layer interference are suitable to enhance the two-color iridescence because the largest peak shift is obtained when the locus crosses the gray zone. However, to satisfy these conditions, it is necessary to strictly control the thickness of the cortex layer, because if the layer is thicker, the locus only moves near the gray zone and then no particular color sense is stimulated, while if it is thinner, the loci draw a circle like an ordinary iridescent thin film (see figure 22). Two-color iridescence is more effective to avian tetrachromatic vision, because the color matching functions in avian vision are much more well-defined owing to the presence of a color filter (oil drop).

5.1.4. Varieties of multilayered structures. Multilayered structures are widely distributed in the animal kingdom [2, 3, 4, 6, 89, 90] and even in the plant kingdom [91], which may include so-called animal reflectors such as butterfly pupa [6, 92, 93, 94], animal eyes [25, 95, 96] and the external surface of fish [97]. Butterflies and moths are a treasure chest for multilayer interference. Mason [17] already reported a schematic illustration of the scale of a moth of the family Uraniidae using an optical microscope. He found that the multilayer was located at the lower part of the scale parallel to its plane and 5–15 films were found to be present. This finding was confirmed later by transmission electron microscopic (TEM) observations made by Lippert and Gentil for *Urania ripheus* (*Chrysiridia rhipheus*) [41], and by Ghiradella for *Urania fulgens* [43].

We have also investigated the wing of *C. rhipheus* (figure 23) [98, 99] in detail using an optical microscope and have found a peculiar reflection pattern on the arranged scales, which differs considerably from that of the *Morpho* butterfly. In fact, under epi-illumination, neighboring scales constitute a narrow reflective band running laterally, which forms separate parallel bands over a wing (figure 23). It is also noticed that a broad band with different hues covered the area between these narrow bands. Since the scale-sized patterns are too small to discriminate, a mixture of these colors occurs in our eyes. Thus this moth exhibits a kind of color mixing in the wing.

Optical and electron microscopic observations of the longitudinal cross section show that the distal part of the cover scale is strongly curved to make a hemisphere (figure 23), while in the proximal part they are rather flat, where the hemisphere part of an adjacent scale overlaps. Owing to this structure, the two scales form a valley-like deep groove between them. Under TEM observation, the multilayered structure is clearly seen, as shown in figure 23, which is also curved along the surface of the scale. There are six layers at the top of the scale with the number decreasing to two toward the proximal part. The thickness of the dark layer is 170 ± 20 nm, while the clear layer is somewhat distributed from 100 to 150 nm. A detailed analysis shows the color mixing is actually an inter-scale phenomenon due to a specialized form of the overlapping curved scales, and is attained by multilayer reflection. Further this color mixing is strongly polarization-sensitive even under illumination by unpolarized light, because it employs the difference in the reflectivity for naturally existing s- and p-polarized light.

Quite a similar effect, but occurring within a scale, was reported by Vukusic *et al* in the wing of an Indonesian green butterfly, *Papilio palinurus* [100–102]. The green scale of this butterfly shows a 2D array of concavities with 4–6 μm in diameter and 0.5–3 μm in depth. Below a round concavity, a similar curved multilayer consisting of about 20 alternate layers of cuticle and air is present. When white light is incident on this structure, yellow light hitting directly on the bottom of a concavity is selectively reflected, while blue light hitting the side of the concavity is reflected, hits again on an opposite side of the concavity wall and is then reflected back in the reverse direction. Thus, only yellow and blue colors are selectively reflected, which produces green color by color mixing in the eyes.

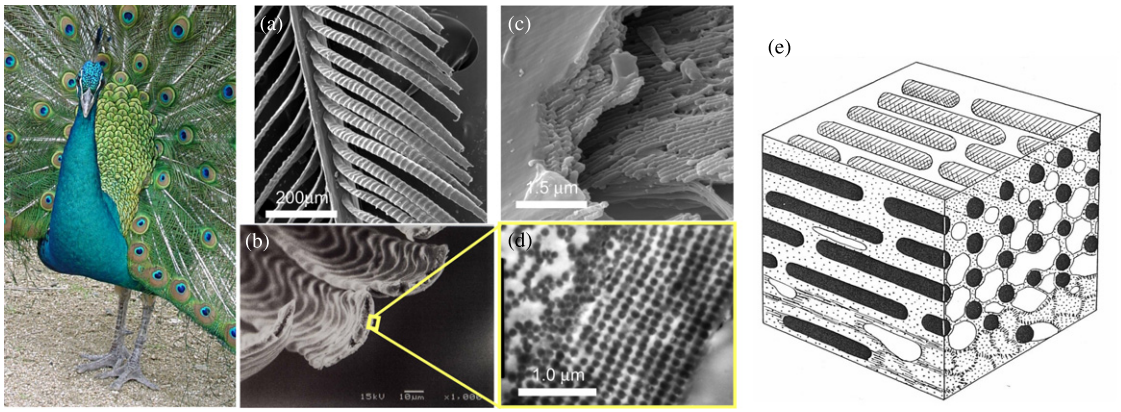

Figure 24. Peacock (Indian peafowl). SEM images of (*a*) barbules, (*b*) the cross section and (*c*) interior of a barbule. (*d*) TEM image of the cross section of a barbule [112]. (*e*) Schematic illustration of a 2D photonic crystal in a peacock barbule (reproduced from [111] with permission).

Probably the most exciting multilayer system is that found in the iridophore of teleosts. The light-induced color changes in this species were first reported by Foster on the male killiefish, whose patches changed from blue or green to orange or wine red within 5 s under light illumination [103]. Similar color changes were reported for cardinal tetra [104] and neon tetra [27, 106–110]. In the iridescent cells of neon tetra, regular arrays of very thin guanine crystals of about 5–10 nm thickness were known to be present [27, 105, 106, 108, 110]. Each cell contained two rows of parallel platelets and simultaneously changed their inclination angles, giving rise to the alteration of the distance between the platelets [108, 110]. This change was found to be induced by light illumination and the change in osmolarity. Nagaishi *et al* [108] called this phenomenon the *venetian blind mechanism* and suggested that the tubulin–dynein interactions played a decisive role in the movement of the platelets. Thus the structural color in this case should be called a dynamical one, whose selected color changes according to the change in the environment. Guanine crystals are known to have a high refractive index of 1.83 and thus only 20 layers of crystal plates of 5 nm thickness give 40% reflectivity. However, the calculated spectral width is unexpectedly sharp owing to an extremely non-ideal character of the multilayer, which differs considerably from experiments.

5.2. *Biological photonic crystals*

5.2.1. Peacock. Photonic crystals are another important source of structural colorations and have been particularly studied in birds and insects. A representative animal possessing this type of structure is the well-known peacock. The feather of the peacock has been attracting scientific attention for more than 300 years. After the early observations by Hooke [7] and Newton [8], it was in the 20th century that detailed observations were made by Mason in 1923 [15]. A feather of the peacock consists of many barbs sticking out from a main shaft and each barb has a lot of barbules. The barbules are curved along their long axis and slightly twisted from the roots. Each barbule has the shape of connected segments of a typical size of 20–30 μm, the surfaces of which are smoothly curved like a saddle. Mason noticed that liquids with a refractive index between 1.55 and 1.60 destroyed the iridescent color most effectively. He considered the origin of the structural coloration to be due to the thin color-producing films of a laminated or plate-like structure.

The sophisticated color-producing structure in a peacock's feather was later clarified by Durrer in 1962 [111] using an electron microscope as illustrated in figure 24(*e*). He reported that the cortex surface layer of the barbule consisted of keratin, within which melanin rods of 1 μm length were arranged in a plane parallel to the surface along the longitudinal direction. Below this plane, a total of 3–11 layers containing the melanin rods were arranged to form a 2D quasi-square lattice. The melanin rods were bound to each other by a keratin band. At the centre of each square lattice, an air hole was located with increasing size toward the lower layer. The medullary region of the barbule was filled with keratin filament with a small number of melanin rods and air holes. He found that the rod separation perpendicular to the surface correlated with the apparent color of the feather, while that parallel to the surface did not show such a correlation.

In figures 24(*a*)–(*d*), we show the barbules observed by SEM. The transverse cross section of a barbule is crescent-shaped (figure 24(*b*)). Under high magnification, 8–12 layers consisting of periodically arrayed particles are observed beneath the surface layer (figure 24(*d*)), whose diameters are in the range 110–130 nm. The layer intervals are actually dependent on the color of the feather: 140–150, 150 and 165–190 nm for blue, green and yellow feathers, respectively [112–114]. It is also noticed that the crescent-shaped barbule makes the lattice structure curved along the surface. In contrast to the transverse section, the particles in the longitudinal direction have a long shape with a length of 0.7 μm and are rather randomly distributed (figure 24(*c*)). These slender particles are melanin granules and cause the barbule to appear dark brown when one looks through it.

Zi *et al* [113] reported detailed calculations on this complicated structure. They employed a barbule of a green peafowl, *P. muticus*, and observed its microstructure using SEM. They calculated the photonic band structure and found a partial band gap along the Γ–X direction for two polarization directions. They also reported the reflection

spectra for blue, green, yellow and brown barbules under a microspectrophotometer and found sharp peaks located at 440 nm and 530 nm for the former two, respectively, while rather broad peaks with side peaks in a blue region for the latter two, indicating that the yellow and brown colors were non-spectral colors. They calculated the reflection spectra for the finite number of lattice planes with a complex refractive index for melanin rods and found fairly good agreement with experiments. Further, they paid particular attention to a brown barbule and found that even the brown color was of a structural origin [115].

These calculations, however, do not essentially reproduce the actual appearance of the peacock's feather. For example, the angular dependence of the reflectivity cannot be explained if the crescent-shaped barbule structure superposed by the lattice structure is not taken into account. We have measured the angular dependence of the reflection spectrum with changing size of the illuminated area [112,114]. When several barbs are illuminated, the reflection spectra are found to be quite smooth and tend to shift toward the blue color with the changing angle of the reflection, while the reflection spectra are rather irregular and the angle-dependent spectral shift is less distinct when a single barbule is illuminated. We have performed the calculation to reproduce the angular dependence taking into account the variation in the macroscopic scale. For this purpose, we introduce the variation of the lattice direction by assuming a Gaussian distribution for the tilt angle of the lattice. The calculated results seem to be in fairly good agreement with the experiment performed on several barbs. The tilt-angle distribution may partly reflect the crescent-shape cross section of a barbule and partly the curved and twisted forms of the barbule. Thus, both the regularities due to the photonic crystal and the macroscopic arrangement are essentially necessary to reproduce the actual appearance of the peacock.

5.2.2. Other birds. Structurally colored barbules in avian species are normally composed of well-ordered melanin granules. These granules originally cause the black, gray and brown colors in the feather, but play an important role in displaying structural colors by arranging into a regular structure and also enhancing its color by acting as a background absorber.

The sophisticated structure in feather barbules was first observed under an electron microscope by Greenewalt *et al* for humming birds [22]. They found the presence of platelet mosaics on the barbules in nearly 50 species of humming birds under an optical microscope. The platelets were of an elliptic shape of 2–3 μm length and 1–1.5 μm width. They further measured the reflection spectrum and found that a sharp peak appeared in the visible region with a width of 60–90 nm, the maximum reflectivity of which amounted to 50%. The electron microscopic observations showed that 7–15 layers of discrete platelets lay parallel to the surface. The platelet consisted of air voids sandwiched by melanin layers and was divided into pieces reminiscent of a 'monolayered foam'. The thickness ranged from 100 to 220 nm. They considered that the platelet constituted a half-wave interference plate by changing the thickness of air voids to accommodate the specific color. They analyzed the origin of the extraordinarily narrow reflection spectrum in terms that the refractive index of the melanin layer changed smoothly within a platelet.

Later, Durrer [116,117] reported systematic investigations on the iridescent barbules and classified the shapes and arrangement of melanin granules. He classified the shapes of the melanin granules into five types: (1) S-type (rod-shaped granule), (2) St-type (thin rod-shaped granule), (3) P-type (flattened stick), (4) R-type (hollow tube) and (5) K-type (platelet like a humming bird). Further, the arrangements of the melanin granules were categorized into five types: (1) E-type (monolayer), (2) K-type (close packing), (3) S-type (multilayer), (4) G-type (lattice type) and (5) O-type (surface layer). So far, a total of 106 iridescent avian species have been classified into 19 categories. For example, the peacock is categorized into the StG-type. Most of the pheasants and ducks belong to the StK-type, while quetzals to the KS or RS-type, hummingbirds to the KK-type, doves to the StS-type except for the rock dove, birds-of-paradise to the StS-type and sunbirds to the PS-type. Thus, at the present stage, the arrangements of melanin granules in barbules have been well systematized. However, the exact interpretations for the color production mechanisms have not been reported. Further systematic studies using modern technology and calculations are clearly needed.

5.2.3. Butterflies and weevils. A small butterfly, *Callophrys rubi*, widely distributed from Europe to Asia and North Africa, first received attention in 1921 [12]. Onslow noticed that the scale of this butterfly was covered with irregular polygonal dark patches when observed under transmitted illumination. Each polygonal area was rimmed by bright lines. Under reflected light, the scale showed green spangles, which corresponded to the dark areas in the transmission.

Schmidt [118] called this type of scale with irregular patches the 'mosaic scale' and investigated a similar scale of *Teinopalpus imperialis* under an optical microscope. He speculated the cause of the structural color in the scale as being due to a lattice consisting of obliquely running thin lamellae. The microstructure of this mosaic scale was later investigated through an electron microscope by Morris in 1975 [119]. He observed that the polygonal grain, seen as a mosaic patch, was 5.4 μm in mean diameter and each consisted of a simple cubic network with hollow spheres at lattice points, which were arranged in a closed-packed cubic (fcc) structure [43,120] with a lattice constant of 0.257 μm.

Thus, the elaborate structure in the interior of the scale in *C. rubi* is now well known as a typical example of biological photonic crystals of an air-hole type. Similar structures were found in *C. siva* [121], *C. avis* [122], *Mitoura grynea* [30, 44] and *Thecla damo* [30]. Ghiradella [29] reported developmental studies on the lycaenid species, *M. grynea*, which possessed crystalline structure in the lower part of the scale. She performed electron microscopic observations during pupal periods of this butterfly. At first, the scale showed a similar architecture often seen in ordinary scales, but on the eighth day after pupation, the internal specialization

began: the combination of the membrane surrounding a core of nascent cuticle formed a unit, aggregated into a lattice forming small crystallites and then formed a quite regular arrangement of a closed-packed lattice structure by accretion. The enclosing membrane–cuticle units were connected with each other and also with the outer space and thus essentially had an extracellular character. The formation process of the lattice continued for two days and the structure became firmly fixed in position as the cell died back and disappeared.

Among various scale-bearing beetles, weevils are quite interesting subjects for studies on structural coloration. Michelson [10] investigated a weevil called diamond beetle, possibly *Estimus imperialis*, which possessed brilliant and exquisitely colored scales on the elytron. Since the color distinguished when the scale was immersed into liquid and further the reflection color was not widely distributed, he considered that the color of this beetle was due to the fine striations on the interior surface of the scale and had an unsymmetrical saw-tooth shape, which was intended to enhance a particular diffraction order. Onslow [123] found a well-defined crossed appearance like the strings of a tennis racquet when viewing the cross section of the scale of *E. imperialis* and opposed to Michelson's specially designed grating.

About 60 years later, Ghiradella [42] found very peculiar structures within a scale of local weevil, *Polydrusus sericeus*. The scale of this beetle possessed a similar lattice structure reminiscent of the scale of a butterfly, *C. rubi*. Later, she described that it was a space lattice that diffracted light to produce a sparkling green color very similar to that of sunlit leaves [45]. Parker *et al* [124] reported that *Pachyrhynchus argus* found in the forests in northeastern Queenland, Australia, showed a metallic coloration visible from any direction owing to a photonic crystal analogous to opal. They reported that within a weevil's scale, many transparent spheres of 250 nm diameter constituted a photonic crystal of hexagonal closed-packing and selectively reflected 530 nm light. Further, they considered that the domain structure within a scale contributed to the omnidirectional color.

Thus, nowadays, the structural colorations due to photonic-crystal-type elaborations are widely known and have become one of the most popular structures. In fact, similar structures are found at various phylogenetic levels of the animal kingdom such as the sea mouse [125, 126], the jelly fish [127] and even in viruses [128]. However, the theoretical model of this type of structure to derive the optical properties remains within a too simplified model calculation such as the photonic band calculation applied to a crystal of an infinite size and the reflection/transmission calculation applied to the regular structure, which are far different from what we need to correctly express the true appearances of these animals. Thus, a simple but universal model to explain their optical characteristics and a general explanation for the formation processes are strongly needed from a physical approach.

5.3. Non-iridescent colorations

Scattering of light is the other source of structural colors, which is completely different from multilayer interference and the photonic-crystal type, because it has an origin in the irregularity of the structure. Light scattering has been considered a cause of blue coloring in a wide variety of random media. The origin of the blue sky was explained first by Lord Rayleigh as being due to light scattering by atmospheric molecules. The color of the suspension involving small colloidal particles is called Tyndall blue. The blue colors in these cases are based on the fact that the scattering cross section is dependent on the fourth power of the light frequency. With increasing size of the particle, Mie scattering occurs, whose wavelength dependence differs considerably from Rayleigh scattering. Thus a different color appears.

Light scattering has often appeared in the literature as a typical example of the non-iridescent structural colors. Mason [14, 16] reported that the colors of some birds and insects were due to Tyndall blue and exemplified the feather of a blue jay and the body and wing of dragonflies. He considered six necessary conditions for a medium to give Tyndall blue: (1) inhomogeneities in the refractive index, (2) dimensions comparable to the wavelength of light, (3) blue scattering and red transmission, (4) size-dependent depth of blue, (5) polarized scattering and (6) inverse proportionality to the fourth power of the wavelength. Huxley [129] suggested that the color of the blue scale in an African butterfly, *Papilio zalmoxis*, is partly due to Tyndall scattering at a layer of air-filled alveoli and partly due to the thin-film interference at a basement lamella. In 1939, the first electron microscopic observation was done by Frank and Ruska [19] to clarify the mechanism of blue coloring in the feathers of the ivory-breasted pitta. They found a spongy structure consisting of keratin and air at the medullary cell wall and assigned it as an origin of Tyndall scattering. Ghiradella [30] also referred to the butterfly scale of *P. oribazus* as being due to Tyndall blue. Parker *et al* [130] explained the gradation from blue to white in terms that the relative sizes of particles determined the shade of blue. He exemplified the wing and body of dragonflies as being due to Tyndall scattering caused by minute colorless granules within epidermal cells located over a dark base. In spite of these descriptions, there had been no report to accurately measure the wavelength dependence of the scattering cross section and its polarization characteristics. Thus, the problem of whether pure Rayleigh/Tyndall scattering determined the colors of animals or not was somewhat behind the veil.

However, it has been gradually recognized that light scattering is somehow organized and contributes effectively to animal colors. For example, the spongy medullary keratin matrices found in the feather barb of birds such as the parakeet and the cotinga had been widely believed to be due to Rayleigh scattering. However, this model failed to explain their reflection spectra because they have a peak from the violet to the blue region. The first report on the presence of interference phenomena was by Raman [131], who cast doubt on Tyndall scattering in a feather of an Indian roller

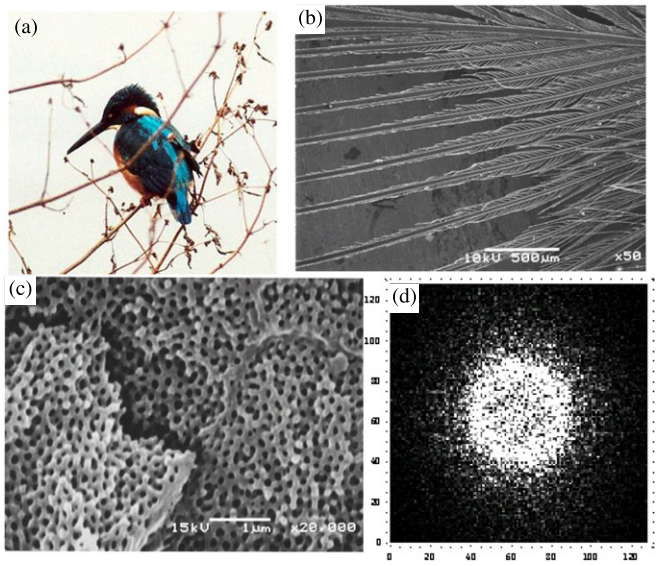

Figure 25. (*a*) Common kingfisher and (*b*) its feather barbs observed under SEM. (*c*) The SEM image of the cross section of a barb and (*d*) the spatial Fourier transformation of the TEM image of the cross section of a barb [6].

and suggested the possibilities of light diffraction from not a small cavity or the interference due to a film. Later, the cause of non-iridescent violet, blue and green barbs was found to be due to the keratin matrix structure in medullary cells in a barb from electron microscopic observations. Dyck [132–134] called it a 'spongy structure', which consisted of a three-dimensional network of keratin rods of 0.1 μm diameter and air channels of 0.1 μm width between them (see figure 25(*c*)). Although the rods and channels were strikingly uniform in size, their orientations were clearly random. Dyck measured the reflection spectra of violet, blue and green barbs of three structurally colored avian species and found a clear peak from the ultraviolet to the visible regions. Further he found that the sizes of the keratin rods and air channels varied in strong correlation with the reflection color. Thus, it was clear that a simple model based on Tyndall scattering was no longer applicable to these systems. He proposed a 'hollow cylinder model' to explain the interference phenomena. However, the agreement with experiments was not satisfactory.

Along this stream, Prum *et al* [135–139] performed a spatial Fourier transformation of the TEM image of the spongy structure and found a clear ring structure in momentum space. If spongy structure with a wide variety of sizes was distributed, a Gaussian-like distribution would be obtained. The presence of a ring structure clearly means that the uniform characteristic size of the matrix actually exists. This situation is easily reproduced by placing randomly oriented broken multilayers, whose layer thicknesses are coincident with the widths of the air channel and the keratin rod, respectively. It is clear that the medullary keratin matrix functions to produce brilliant hues in a similar way to multilayer reflectors, but the reflection is nearly omnidirectional. They also examined similar structures in avian skins of various species [140, 141], which appeared as quasi-ordered arrays of parallel collagen fibers, and found a similar spatial order.

It is now clear that a simple model based on Rayleigh/Tyndall scattering fails to explain the non-iridescent blue colorations, since a definite peak is observed in the reflection spectrum and also a clear spatial correlation exists in seemingly random structures. It appears that these structures are widely distributed in the animal world, particularly in birds (see, for example [139]) and insects [6, 122, 137, 142, 143]. Their structural units appear sometimes in the form of a network, stacks having random holes and sometimes randomly distributed spheres. These findings are quite important because the structures actually possess uniform characteristic length, which changes the incoherent scattering into coherent scattering, enforcing reflection to a large extent. Although the 2D Fourier transform method has been widely used to find the spatial correlation within seemingly random structures, problems still remain unsolved. Prum *et al* attempted to combine the 2D Fourier images with the reflection spectrum using an average refractive index calculated from the areas of keratin rods and air channels. However, this treatment essentially neglects multiple scattering, which is essential to cause the interference of light within a regularly arranged structure and hence to produce a highly reflective band in the reflection spectrum. Thus in spite of the usefulness and easiness of the 2D Fourier method, it should always be kept in mind that the 2D Fourier image reflects the scattering field only in a limited sense.

6. Summary and outlook

We have overviewed structural colors in various animal orders and have attempted to derive the essential features of their color-producing structures. Clearly, not only the regular structure but also irregularity on the order of the wavelength of light plays an important role in their appearance. The former is primarily essential to strongly reflect the light through interference, while the latter is inevitable to diffuse it in an omnidirectional way. Evidently, these two factors cooperate properly to give a maximal effect for the animal's purpose. An extreme case is an animal reflector, which gives almost complete specular reflection, and thus only the former plays a decisive role. On the other hand, if the latter plays a role, and yet the former effect is still much stronger, the structural color gives a strong color impression to the surroundings. A good example is the *Morpho* butterfly, which employs anisotropic reflection to restrict the direction of the reflection within a 2D plane and emits strong *Morpho* blue in specific directions. A completely different way of coloring is based on non-iridescent coloring, in which the irregular structure plays a central role and produces a moderate intensity of coloring.

In some cases, in addition to such irregularity, animals employ special structures on a macroscopic scale, within which the coloring mechanisms are enclosed, to diffuse the reflection of light effectively. Typical examples are the crescent shape of a barbule in a peacock and the alveoli on the elytron of a tiger beetle. These structures make the direction of the reflection broader by altering the incidence plane and angle. The size of such structures generally lies within the range 10–30 μm.

On the other hand, many animals possess characteristic structures or their arrangements of a much larger size. Examples are barbs in feathers, scales in butterflies, holes in beetles' elytra and so on. At a glance, these structures have no relation to structural coloration, because their sizes are too large to give any coloring effect. However, as implied in experiments on the peacock feather or on the *Morpho* wing, these structures give a special effect that cannot be expressed in terms of known optical characteristics such as spectral distribution, angular dependence and polarization. It should be called the *texture* of a material such that silk looks like silk and cotton looks like cotton.

We believe that the texture of a material is deeply connected with such macroscopic structures or their arrangements. We can find a simple example in Japanese painting, which is often drawn using mineral pigments (grains made by grinding various colored stones). These pigments are mixed with dilute glue to make coloring materials. Thus the pigments laid on the painting look like grains scattered on a sheet of paper, which are visible to the naked eye when one sees them close up. However, when seeing from a distance, one abruptly senses the texture of the painted material such that a painted tree just looks like a real tree although it is made only from colored grains. This effect should be called *coarse graining*, by which animals may display their own specific texture. The macroscopic structure such as the scale arrangement on a butterfly wing will surely benefit from expressing such a texture. Thus structural colors should always be considered from the viewpoint of how they are seen both in the microscopic and in the macroscopic scales.

Actually, many problems are left unresolved concerning the optical properties of complex structures in order to truly understand structural colors in nature. These include (1) optical responses from regular structures when the irregularity is actively incorporated, (2) those due to irregularity-based structure to give non-iridescent colors, (3) effect of the macroscopic shape on the coloration, (4) coarse graining effect using the macroscopic arrangement and (5) complex interaction between pigment and nanostructure.

Finally, we briefly mention how these structures are created in the natural environment. As we have described above, developmental studies on the color-producing structures have been extremely limited up to now. Ghiradella [28] investigated the development of ultraviolet-reflecting butterfly scales in pupa and found that prior to the cuticle secretion, the bundles of microfilaments were distributed specifically and that the succeeding cuticle secretion seemed to follow it. Further, she assumed that the mechanical stress was imposed on the cuticle projection and caused elastic buckling, which resulted in the shelf structure. In a tiny butterfly *Mitoura grynea*, the arrangement of the cylindrical sleeve of membrane surrounding the core of the nascent cuticle was recognized before generating the photonic-crystal type structure [29]. Thus before the microstructure is created, regular distributions of nascent structures seem always necessary.

Such regular structures, stationary in time and inhomogeneous in space, are likely to come from a kind of instability occurring in a reaction–diffusion system [144, 145]. Turing proposed that morphogenesis in a living thing was formed through kinetic processes in chemical reactions. Consider a simple 1D model system consisting of two components, activator u and inhibitor v. The concentrations of these components are generally expressed by the following reaction–diffusion system: $\partial u/\partial t = D_u \partial^2 u/\partial x^2 + f(u, v)$ and $\partial v/\partial t = D_v \partial^2 v/\partial x^2 + g(u, v)$, where D_u and D_v are diffusion coefficients for u and v, respectively, and $f(u, v)$ and $g(u, v)$ are reaction terms. The stability of the solutions of these equations is easily investigated through linearized stability analysis, in which the small spatial modulations on the concentrations with the wavenumber of q, are posed on the uniform solutions of $\bar{u}$ and $\bar{v}$ as in the form of $u = \bar{u} + a\exp(\lambda t + \mathrm{i}qx)$ and $v = \bar{v} + b\exp(\lambda t + \mathrm{i}qx)$. After some calculations, the following relation is obtained to evaluate the stability of the system: $\lambda^2 + A(q)\lambda + B(q) = 0$, where $A(q) = q^2(D_u + D_v) - (f_u + g_v)$ and $B(q) = D_u D_v q^4 - q^2(D_u g_v + D_v f_u) + f_u g_v - f_v g_u$. $f_{u,v}$ and $g_{u,v}$ are the coefficients of the partial derivative with respect to u and v for the uniform solutions, where in the activator–inhibitor system, the relations $f_u > 0$, $f_v < 0$, $g_u > 0$ and $g_v < 0$ are generally assumed.

For $q = 0$, the uniform solutions $\bar{u}$ and $\bar{v}$ require $f_u + g_v < 0$ and $f_u g_v - f_v g_u > 0$ for the linearized stability. For $q \neq 0$, the condition $B(q) < 0$ gives a positive value of λ, which results in the instability of the uniform solutions in a particular range of q, causing stable spatial modulation under stationary conditions. To estimate the value of q, we consider q_c, giving the minimum value of $B(q)$, which is given as $q_c^2 = (D_u g_v + D_v f_u)/2D_u D_v$ with $B(q_c) = -(D_u g_v + D_v f_u)^2/(4D_u D_v) + f_u g_v - f_v g_u$. Close inspection shows that in order to attain $B(q_c) < 0$, it is necessary that D_u takes a very small value if D_v is kept constant. Thus a large difference in the diffusion constants for the activator and inhibitor causes spatial instability in a finite wavenumber. This phenomenon is called *Turing instability* and has recently been confirmed experimentally in reaction–diffusion systems [146, 147].

Under the condition that $-g_v D_u \ll f_u D_v$, the above relation reduces to $q_c \approx (f_u/D_u)^{1/2}$, which offers the relationship between the pattern size and the reaction rate/diffusion coefficient. If we apply this relation to color-producing structures, we can estimate the necessary condition to create the microstructures. Since the reaction rate is not known, for the present, we obtain only the diffusion coefficient with the help of recently reported reaction–diffusion systems. For example, employing the values $D_u \approx 10^{-9}\,\mathrm{m^2\,s^{-1}}$ and $q_c \approx 10^4\,\mathrm{m^{-1}}$ for a gel reactor [148], we have estimated the diffusion constant for our case as $D_u \approx 10^{-15}\,\mathrm{m^2\,s^{-1}}$ for $q_c \approx 10^7\,\mathrm{m^{-1}}$. Thus, the diffusion coefficient required for creating the color-producing pattern is estimated to be 7 orders of magnitude smaller than that in water. Although the difference in the reaction rates may largely affect the result, it partly explains why complex chemical structures such as cuticle or keratin are actually used to create the microstructures. Thus, in the near future, it will be extremely important to construct a model system to investigate the formation process within a laboratory environment, where the experimental conditions are completely controlled.

References

[1] Parker A R 1998 *J. Exp. Biol.* **201** 2343–7
[2] Srinivasarao M 1999 *Chem. Rev.* **99** 1935–61
[3] Parker A R 2000 *J. Opt. A: Pure Appl. Opt.* **2** R15–R28
[4] Vukusic P and Sambles J R 2003 *Nature* **424** 852–5
[5] Parker A R 2004 *Phil. Trans. R. Soc. Lond.* A **362** 2709–20
[6] Kinoshita S and Yoshioka S 2005 *ChemPhysChem* **6** 1442–59
[7] Hooke R 1665 *Micrographia: Or Some Physiological Descriptions of Minute Bodies made by Magnifying Glasses with Observations and Inquiries thereupon* (New York: Dover 1961)
[8] Newton I 1704 *Opticks: Or, a Treatise of the Reflections, Refractions, Inflections and Colours of Light* (New York: Dover 1952)
[9] Lord Rayleigh 1919 *Phil. Mag.* **37** 98–111
[10] Michelson A A 1911 *Phil. Mag.* **21** 554–66
[11] Lord Rayleigh 1917 *Proc. R. Soc. Lond.* A **93** 565–77
[12] Onslow H 1923 *Phil. Trans.* **211** 1–74
[13] Merritt E 1925 *J. Opt. Soc. Am. Rev. Sci. Instrum.* **11** 93–8
[14] Mason C W 1923 *J. Phys. Chem.* **27** 201–51
[15] Mason C W 1923 *J. Phys. Chem.* **27** 401–47
[16] Mason C W 1926 *J. Phys. Chem.* **30** 383–95
[17] Mason C W 1927 *J. Phys. Chem.* **31** 321–54
[18] Mason C W 1927 *J. Phys. Chem.* **31** 1856–72
[19] Frank F and Ruska H 1939 *Naturwissenschaften* **27** 229–30
[20] Anderson T F and Richards A G Jr 1942 *J. Appl. Phys.* **13** 748–58
[21] Gentil K 1942 *Z. Morph. Ökol. Tiere* **38** 344–55
[22] Greenewalt C H, Brandt W and Friel D D 1960 *J. Opt. Soc. Am.* **50** 1005–13
[23] Neville A C and Caveney S 1969 *Biol. Rev.* **44** 531–62
[24] Durrer H and Villiger W 1972 *Int. J. Insect Morphol. Embryol.* **1** 233–40
[25] Land M F 1972 *Prog. Biophys. Mol. Biol.* **24** 75–106
[26] Bernhard C G, Gemne G and Møller A R 1968 *Q. Rev. Biophys.* **1** 89–105
[27] Lythgoe J N and Shand J 1982 *J. Physiol.* **325** 23–34
[28] Ghiradella H 1978 *J. Morph.* **142** 395–410
[29] Ghiradella H 1989 *J. Morph.* **202** 69–88
[30] Ghiradella H 1991 *Appl. Opt.* **30** 3492–500
[31] Schultz T D and Rankin M A 1985 *J. Exp. Biol.* **117** 111–7
[32] Yin H, Shi L, Sha J, Li Y, Qin Y, Dong B, Meyer S, Liu X, Zhao L and Zi J 2006 *Phys. Rev.* E **74** 051916
[33] Yoshioka S, Nakamura E and Kinoshita S 2007 *J. Phys. Soc. Japan* **76** 013801
[34] Born M and Wolf E 1975 *Principles of Optics: Electromagnetic Theory of Propagation, Interference and Diffraction of Light* 5th edn (New York: Pergamon)
[35] Kinoshita S and Yoshioka S 2005 *Structural Colors in Biological Systems—Principles and Applications* ed S Kinoshita *et al* (Osaka: Osaka University Press) pp 3–26
[36] Huxley A F 1968 *J. Exp. Biol.* **48** 227–45
[37] Sakoda K 2001 *Optical Properties of Photonic Crystals* (Berlin: Springer)
[38] Fujimura Y 2008 *Thesis* Osaka University submitted
[39] Ackery P R, de Jong R and Vane-Wright R I 1998 *Handbook of Zoology* IV *Arthropoda: Insecta—Lepidoptera, Moths and Butterflies* ed N P Kristensen (Berlin: Walter de Gruyter) pp 263–300
[40] Süffert F 1924 *Z. Morph. Ökol. Tiere* **1** 171–308
[41] Lippert W and Gentil K 1959 *Z. Morph. Ökol Tiere* **48** 115–22
[42] Ghiradella H 1984 *Ann. Entomol. Soc. Am.* **77** 637–45
[43] Ghiradella H 1985 *Ann. Entomol. Soc. Am.* **78** 252–64
[44] Ghiradella H 1994 *Microsc. Res. Tech.* **27** 429–38
[45] Ghiradella H 1998 *Microscopic Anatomy of Invertebrates* vol 11A: Insecta ed F W Harrison *et al* (New York: Wiley-Liss) pp 257–87
[46] Wright W D 1963 *Nature* **4887** 1239–44
[47] Pillai P K C 1968 *J. Opt. Soc. Am.* **58** 1019–22
[48] Cowan J J 1990 *J. Opt. Soc. Am.* A **7** 1529–44
[49] Kumazawa K, Tanaka S, Negita K and Tabata H 1994 *Japan. J. Appl. Phys.* **33** 2119–22
[50] Tabata H, Kumazawa K, Funakawa M, Takimoto J and Akimoto M 1996 *Opt. Rev.* **3** 139–45
[51] Tabata H, Hasegawa T, Nakagoshi M, Takikawa S and Tsusue M 1996 *Cell. Mol. Life Sci.* **52** 85–7
[52] Kumazawa K, Negita K, Hasegawa T and Tabata H 1996 *J. Exp. Zool.* **275** 15–9
[53] Vukusic P, Sambles J R, Lawrence C R and Wootton R J 1999 *Proc. R. Soc. Lond.* B **266** 1403–11
[54] Mann S E, Miaoulis I N and Wong P Y 2001 *Opt. Eng.* **40** 2061–8
[55] Gralak B, Tayeb G and Enoch S 2001 *Opt. Express* **9** 567–78
[56] Kinoshita S, Yoshioka S and Kawagoe K 2002 *Proc. R. Soc. Lond.* B **269** 1417–21
[57] Kinoshita S, Yoshioka S, Fuii Y and Okamoto N 2002 *Forma* **17** 103–121
[58] Berthier S, Charron E and Da Silva A 2003 *Opt. Commun.* **228** 349–56
[59] Yoshioka S and Kinoshita S 2004 *Proc. R. Soc. Lond.* B **271** 581–7
[60] Plattner L 2004 *J. R. Soc. Interface* **1** 49–59
[61] Kinoshita S and Yoshioka S 2005 *Structural Colors in Biological Systems—Principles and Applications* ed S Kinoshita *et al* (Osaka: Osaka University Press) pp 113–40
[62] Yoshioka S and Kinoshita S 2006 *Proc. R. Soc. Lond.* B **273** 129–34
[63] Wickham S, Large M C J, Poladian L and Jermiin L S 2006 *J. R. Soc. Interface* **3** 99–109
[64] Berthier S, Charron E and Boulenguez J 2006 *Insect Sci.* **13** 145–57
[65] Prum R O, Quinn T and Torres R H 2006 *J. Exp. Biol.* **209** 748–65
[66] Banerjee S, Cole J B and Yatagai T 2007 *Micron* **38** 97–103
[67] Yoshioka S, Kinoshita S and Saito A 2004 *Oyo Butsuri* **73** 939–42
[68] Saito A, Yoshioka S and Kinoshita S 2004 *Proc. SPIE* **5526** 188–94
[69] Penz C M and DeVries P J 2002 *American Museum Novitates* vol 3374 (New York: The American Museum of Natural History) pp 1–33
[70] Iohara K, Yoshimura M, Tabata H and Shimizu S 2000 *Chem. Fibers Int.* **50** 38–9
[71] Saito A, Miyamura Y, Nakajima M, Ishikawa Y, Sogo K, Kuwahara Y and Hirai Y 2006 *J. Vac. Sci. Technol.* B **24** 3248–51
[72] Matsui S, Kaito T, Fujita J, Komuro M, Kanda K and Haruyama Y 2000 *J. Vac. Sci. Technol.* B **18** 3181–4
[73] Hoshino T *et al* 2003 *J. Vac. Sci. Technol.* B **21** 2732–6
[74] Watanabe K, Hoshino T, Kanda K, Haruyama Y and Matsui S 2005 *Japan. J. Appl. Phys.* **44** L48–50
[75] Watanabe K, Hoshino T, Kanda K, Haruyama Y, Kaito T and Matsui S 2005 *J. Vac. Sci. Technol.* B **23** 570–4
[76] Lord Rayleigh 1923 *Proc. R. Soc. Lond.* A **103** 233–9
[77] Lord Rayleigh For Sec R S 1930 *Proc. R. Soc. Lond.* A **128** 624–41
[78] Schultz T D and Rankin M A 1985 *J. Exp. Biol.* **117** 87–110
[79] Schultz T D 1986 *Bull. Entomol. Soc. Am.* **32** 142–6
[80] Kurachi M, Takaku Y, Komiya Y and Hariyama T 2002 *Naturwissenschaften* **89** 295–8
[81] Hariyama T, Hironaka M, Horiguchi H and Stavenga D G 2005 *Structural Colors in Biological Systems—Principles*

and Applications ed S Kinoshita *et al* (Osaka: Osaka University Press) pp 153–76
[82] Bouligand Y 1965 *C. R. Acad. Sci. Paris* **261** 4864–7
[83] Neville A C 1975 *Biology of the Arthropod Cuticle* (Berlin: Springer)
[84] Neville A C 1993 *Biology of Fibrous Composites—Development beyond the Membrane* (Cambridge: Cambridge University Press)
[85] Neville A C, Parry D A D and Woodhead-Galloway J 1976 *J. Cell Sci.* **21** 73–82
[86] Caveney S 1971 *Proc. R. Soc. Lond.* B **178** 205–25
[87] Osorio D and Ham A D 2002 *J. Exp. Biol.* **205** 2017–27
[88] McGraw K J 2004 *Naturwissenschaften* **91** 125–9
[89] Neville A C 1977 *J. Insect Physiol.* **23** 1267–74
[90] Parker A R, McKenzie D R and Large M C J 1998 *J. Exp. Biol.* **201** 1307–13
[91] Lee D W 1997 *Am. Sci.* **85** 56–63
[92] Rothschild M, Gardiner B and Mummery R 1978 *J. Zool., Lond.* **186** 351–8
[93] Steinbrecht R A 1985 *Tissue Cell* **17** 745–62
[94] Steinbrecht R A, Mohren W, Pulker H K and Schneider D 1985 *Proc. R. Soc. Lond.* B **226** 367–90
[95] Land M F 1978 *Sci. Am.* **239** 88–99
[96] Land M F 2000 *J. Opt. A: Pure Appl. Opt.* **2** R44–R50
[97] Denton E J 1970 *Phil. Trans. R. Soc. Lond.* B **258** 285–13
[98] Yoshioka S and Kinoshita S 2007 *Opt. Express* **15** 2691–701
[99] Yoshioka S and Kinoshita S 2007 *J. R. Soc. Interface* **5** 457–64
[100] Vukusic P, Sambles J R and Lawrence C R 2000 *Nature* **404** 457–8
[101] Vukusic P, Sambles R, Lawrence C and Wakely G 2001 *Appl. Opt.* **40** 1116–25
[102] Vukusic P 2005 *Structural Colors in Biological Systems—Principles and Applications* ed S Kinoshita *et al* (Osaka: Osaka University Press) pp 95–112
[103] Foster K W 1933 *Proc. Natl Acad. Sci.* **19** 535–40
[104] Rohrlich S T 1974 *J. Cell Biol.* **62** 295–304
[105] Clothier J and Lythgoe J N 1987 *J. Cell Sci.* **88** 663–8
[106] Lythgoe J N and Shand J 1989 *J. Exp. Biol.* **141** 313–25
[107] Nagaishi H and Oshima N 1989 *Pigment Cell Res.* **2** 485–92
[108] Nagaishi H, Oshima N and Fujii R 1990 *Comp. Biochem. Physiol.* A **95** 337–41
[109] Oshima N and Nagaishi H 1992 *Comp. Biochem. Physiol.* A **102** 273–8
[110] Nagaishi H and Oshima N 1992 *Zool. Sci.* **9** 65–75
[111] Durrer H 1962 *Verhand. Naturforsch. Ges. Basel* **73** 204–24
[112] Yoshioka S and Kinoshita S 2002 *Forma* **17** 169–81
[113] Zi J, Yu X, Li Y, Hu X, Xu C, Wang X, Liu X and Fu R 2003 *Proc. Natl Acad. Sci.* **100** 12576–8
[114] Yoshioka S and Kinoshita S 2005 *Structural Colors in Biological Systems—Principles and Applications* ed S Kinoshita *et al* (Osaka: Osaka University Press) pp 195–208
[115] Li Y, Lu Z, Yin H, Yu X, Liu X and Zi J 2005 *Phys. Rev.* E **72** 10902
[116] Durrer H 1977 *Denkschr. Schweiz. Naturforsch. Ges.* **91** 1–127
[117] Durrer H 1986 *Biology of the Integument* 2 Vergebrates ed J B-Hahn *et al* (Berlin: Springer) pp 239–47
[118] Schmidt W J 1943 *Z. Morphol. Ökol. Tiere* **39** 176–216
[119] Morris R B 1975 *J. Entomol.* A **49** 149–54
[120] Ghiradella H and Radican W 1976 *J. Morph.* **150** 279–98
[121] Allyn A C and Downey J C *Bull. Allyn Museum* **40** 1–6
[122] Tilley R J D and Eliot J N 2002 *Trans. Lepid. Soc. Japan* **53** 153–80
[123] Onslow H 1920 *Nature* **106** 181–3
[124] Parker A R, Welch V L, Driver D and Martini N 2003 *Nature* **426** 786–7
[125] Parker A R, McPhedran R C, McKenzie D R, Botten L C and Nicorovici N A 2001 *Nature* **409** 36–7
[126] McPhedran R C, Nicorovici N A, McKenzie D R, Botten L C and Parker A R 2001 *Aust. J. Chem.* **54** 241–4
[127] Welch V, Vigneron J P, Lousse V and Parker A R 2006 *Phys. Rev.* E **73** 041916
[128] Juhl S B *et al* 2006 *Adv. Func. Mater.* **16** 1086–94
[129] Huxley J 1976 *Proc. R. Soc. Lond.* B **193** 441–53
[130] Parker A R and Martini N 2006 *Opt. Laser Technol.* **38** 315–22
[131] Raman C V 1934 *Proc. Ind. Acad. Sci.* **1** 1–7
[132] Dyck J 1971 *Z. Zellforsch.* **115** 17–29
[133] Dyck J 1971 *Biol. Skrift.* **18-2** 1–67
[134] Dyck J 1976 *Proc. 16th Int. Ornithological Congress (Canberra)* pp 426–37
[135] Prum R O, Torres R H, Williamson S and Dyck J 1998 *Nature* **396** 28–9
[136] Prum R O, Torres R, Williamson S and Goodman S M 1999 *J. Exp. Biol.* **202** 3507–22
[137] Prum R O and Torres R H 2003 *Integr. Comp. Biol.* **43** 591–602
[138] Prum R O, Andersson S and Torres R H 2003 *The Auk* **120** 163–70
[139] Prum R O 2006 *Bird Coloration* ed G E Hill *et al* (Cambridge: Harvard University Press) pp 295–353
[140] Prum R O, Torres R, Kovach C, Williamson S and Dyck J 1999 *Proc. R. Soc. Lond.* B **266** 13–22
[141] Prum R O and Torres R 2003 *J. Exp. Biol.* **206** 2409–29
[142] Prum R O, Cole J A and Torres R H 2004 *J. Exp. Biol.* **207** 3999–4009
[143] Prum R O, Quinn T and Torres R H 2006 *J. Exp. Biol.* **209** 748–65
[144] Epstein I R and Pojman J A 1998 *An Introduction to Nonlinear Chemical Dynamics—Oscillations, Waves, Pattern, and Chaos* (New York: Oxford University Press)
[145] Ohta T 2000 *Physics of Non-Equilibrium Systems* (Tokyo: Shokabo)
[146] Castets V, Dulos E, Boissonade J and De Kepper P 1990 *Phys. Rev. Lett.* **64** 2953–6
[147] Ouyang Q and Swinney H L 1991 *Nature* **352** 610–12
[148] Vigil R D, Ouyang Q and Swinney H L 1992 *Physica* A **188** 17–25